Journal of Medicinal Chemistry

pubs.acs.org/jmc Article

Rational Alteration of Pharmacokinetics of Chiral Fluorinated and Deuterated Derivatives of Emixustat for Retinal Therapy

Eliav Blum,[▽] Jianye Zhang,[▽] Jordan Zaluski, David E. Einstein, Edward E. Korshin, Adam Kubas, Arie Gruzman,* Gregory P. Tochtrop,* Philip D. Kiser,* and Krzysztof Palczewski*

Cite This: *J. Med. Chem.* 2021, 64, 8287−8302 Read Online

ACCESS | Metrics & More | Article Recommendations | Supporting Information

ABSTRACT: Recycling of all-*trans*-retinal to 11-*cis*-retinal through the visual cycle is a fundamental metabolic pathway in the eye. A potent retinoid isomerase (RPE65) inhibitor, (*R*)-emixustat, has been developed and tested in several clinical trials; however, it has not received regulatory approval for use in any specific retinopathy. Rapid clearance of this drug presents challenges to maintaining concentrations in eyes within a therapeutic window. To address this pharmacokinetic inadequacy, we rationally designed and synthesized a series of emixustat derivatives with strategically placed fluorine and deuterium atoms to slow down the key metabolic transformations known for emixustat. Crystal structures and quantum chemical analysis of RPE65 in complex with the most potent emixustat derivatives revealed the structural and electronic bases for how fluoro substituents can be favorably accommodated within the active site pocket of RPE65. We found a close (∼3.0 Å) F−π interaction that is predicted to contribute ∼2.4 kcal/mol to the overall binding energy.

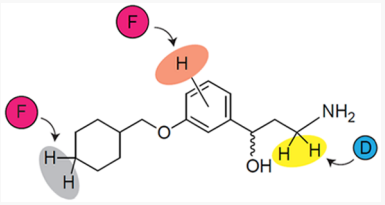

INTRODUCTION

Retinal photoreceptor cells can respond to light throughout life because they continuously regenerate a light-sensitive chromophore and photoreceptor structures. Defects in various proteins involved in these processes cause photoreceptor degeneration.[1] Light detection is mediated by a group of G protein-coupled receptor proteins called opsins located in rod and cone photoreceptor cells of the retina. The light-absorbing chromophore of most vertebrate opsins is 11-*cis*-retinal. Absorption of a photon by an opsin pigment causes isomerization of the chromophore to all-*trans*-retinal. Regeneration of the visual chromophore following light exposure is dependent upon an enzymatic pathway referred to as the visual cycle (Figure 1A).[2] To understand why human vision declines with age, considerable research has been focused on the retina, especially the layer of rod and cone photoreceptor cells that convert light into electrical signals. However, age-related decreases in retinal photoreceptor cell function cannot be explained alone by rod/cone cell loss, abnormal retinal plasticity, or any acute signs of retinal disease. Rather, there are pathological events that take place over time, including the aberrant metabolism of all-*trans*-retinal that can interfere with normal photoreceptor function (Figure 1A). All-*trans*-retinal, when released from rhodopsin, primarily re-enters the visual cycle. However, in some individuals, it can also persist as an unbound potentially toxic aldehyde or react with other molecules to create toxic compounds such as *N*-retinylidene-*N*-retinylethanolamine (A2E) and retinal dimers.[3] These events are thought to contribute to the etiology of blinding diseases such as age-related macular degeneration (AMD) and Stargardt disease.[4]

Various therapeutic strategies have been developed to combat the aberrant metabolism of retinoids including all-*trans*-retinal. One of these involves the inhibition of retinoid isomerase (RPE65), a key enzyme of the visual cycle (Figure 1A), to slow down the generation of all-*trans*-retinal without significantly impairing vision. (*R*)-Emixustat, derived from retinylamine (Figure 1B),[5] is currently undergoing clinical development as a potent RPE65 inhibitor.[6−14] However, the complete suppression of RPE65 activity has undesirable blinding consequences, thus only a narrow concentration range of the drug is tolerable. Effective use of emixustat is further complicated because it is rapidly metabolized,[15−18] limiting the duration of its pharmacological effects. A second strategy is to lower the toxic effects of unbound all-*trans*-retinal and temporarily sequester it by condensation with a primary amine.[19,20] Because most RPE65 inhibitors contain an amino group, they can play a dual role of slowing down the metabolism of all-*trans*-retinal as well as sequestering it.[19]

Here, we describe the synthesis of several derivatives of emixustat, involving the strategic incorporation of deuterium or fluorine to investigate three areas of the emixustat structure that could modulate its potency and metabolism (Figure 1C). Regioselective incorporation of fluorine is known to have a broad range of potential impacts on the properties of small

Received: February 13, 2021
Published: June 3, 2021

https://doi.org/10.1021/acs.jmedchem.1c00279
J. Med. Chem. 2021, 64, 8287−8302

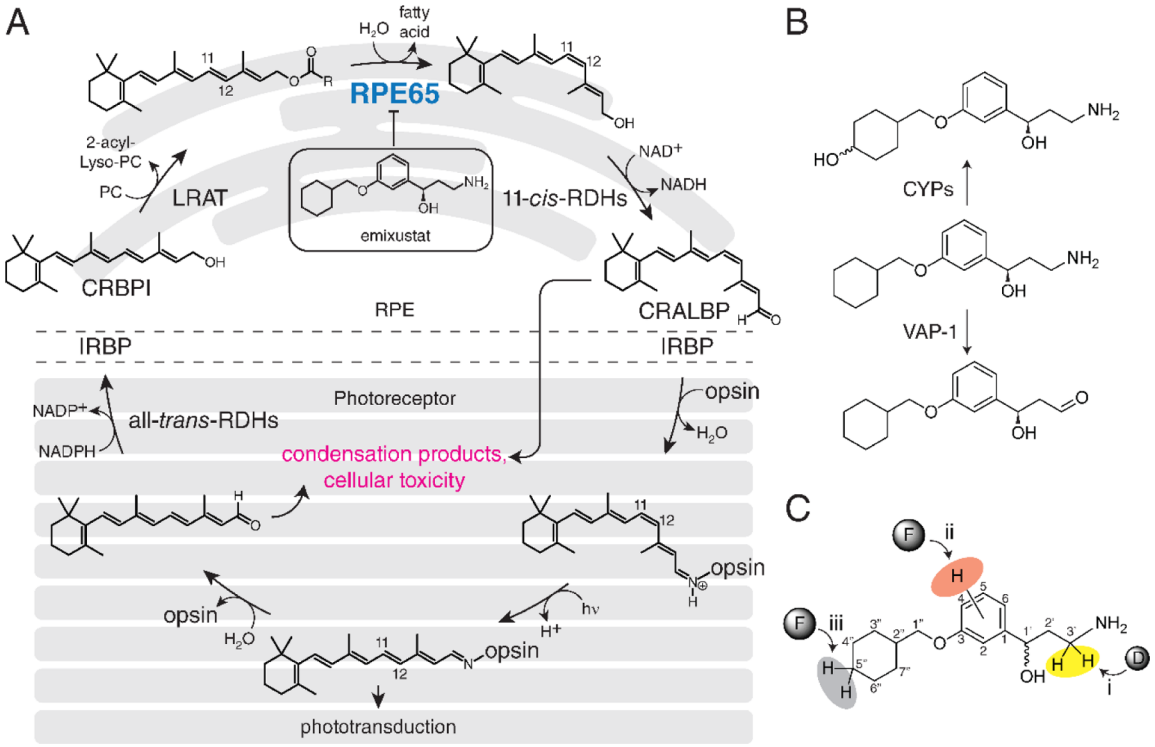

Figure 1. Pharmacodynamics and pharmacokinetics of visual cycle modulators. (A) Visual cycle modulators such as emixustat inhibit RPE65, thus blocking the key *trans*/*cis* isomerization step of the visual cycle and reducing the formation of toxic retinaldehyde condensation products. (B) Sites of emixustat modification *in vivo* and strategies to modify its metabolism. (C) Three strategies for modifying the emixustat metabolism investigated in this work.

molecules. These include pK_a modulation; alteration of target selectivity through conformational variations or changes in specific hydrophobic interactions; and alteration of tissue-specific penetration (e.g., CNS), through modification of lipophilicity.[21] These effects of fluorination are in addition to the well-established strategy of replacing metabolically labile hydrogens with C−F bonds.[22] Regioselective incorporation of deuterium was utilized to investigate the role of amine oxidation in the rapid metabolic elimination of emixustat. We hypothesized that we could attenuate this metabolic process *via* engineering a localized primary isotope effect.[23] Collectively, we envisioned a collection of rationally designed compounds that could improve the potency, absorption, selectivity, and metabolism of drug candidates to mitigate the toxicity of all-*trans*-retinal in age-related blindness.

RESULTS

Synthesis. Here, we report three families of molecules where we employed a common strategy, constructing a variety of alkoxy substituents of a central aryl core initially, and then adding a γ-hydroxyalkylamine moiety, using both established and novel methods. We considered two general approaches that are strategically differentiated by the directionality of molecule assembling with respect to the aryl core (Schemes 1 and 2). Additionally, a possibility of the construction of the chiral γ-hydroxyalkylamine framework with the assistance of removable chiral auxiliary (Scheme 1) as well as an option for intentional α-deuteration toward the amino group (Scheme 2) were considered. In the very beginning of both general synthetic routes, the alkyl substituents were installed onto either a properly fluorinated hydroxyacetophenone (Scheme 1) or a hydroxybenzaldehyde backbone (Scheme 2) through conventional alkylation of the phenolic hydroxyls with the corresponding alkyl bromides or mesylates.

Synthesis of non-racemic (2-propylpentyl)oxyfluorophenyl series of γ-aminoalcohols **23**−**30** by means of capitalization of the chiral removable appendage for the resolution of the diastereomeric intermediates is shown in Scheme 1. Indeed, recently developed for synthesis of enantiopure γ-oxo-α-amino acids[24,25] and β-aminoketones, three-component Mannich reaction with chiral benzylamines[26] being applied to fluorinated in the benzene ring alkoxyacetophenones **1**−**4**, (*S*)-(−)-α-methylbenzylamine and formaldehyde, precursors afforded a suitable access to the corresponding β-aminoketones **5**−**8**. The HCl-catalyzed Mannich reactions of fluorinated acetophenones **1**−**4** with (*S*)-(−)-α-methylbenzylamine leading to the chiral β-aminoketones **5**−**8**, were initially performed using paraformaldehyde and microwave (MW) irradiation (method 1).[27] While this method provided a reasonable yield of β-aminoketones **5** and **7** (47% in both cases) from ketones **1** and **3**, respectively, the reactions of acetophenones **2** and **4** with the ortho-positioned fluoro- and alkoxy-substituents under the MW conditions repeatedly resulted in insufficient production of aminoketones **6** and **8** (<20%). To our delight, the more traditional method of Mannich condensation (heating of **2** and **4** with 1,3,5-trioxane in a sealed pressure tube), method 2,[28] was found to be more efficient for the preparation of chiral β-aminoketones **6** and **8** (34 and 78%, respectively).

The chiral β-aminoketones **5**−**8**, prepared through the Mannich reaction, were reduced by sodium borohydride in MeOH to give the corresponding N-protected γ-aminoalcohols **9**−**12** as a mixture of diastereomers in each case. All of the mixtures of diastereomeric γ-aminoalcohols **9**−**12** could be

https://doi.org/10.1021/acs.jmedchem.1c00279
J. Med. Chem. 2021, 64, 8287−8302

Scheme 1. Synthesis and Asymmetric Resolution of (2-Propylpentyl)oxyfluorophenyl Analogues of Emixustat 23−30[a]

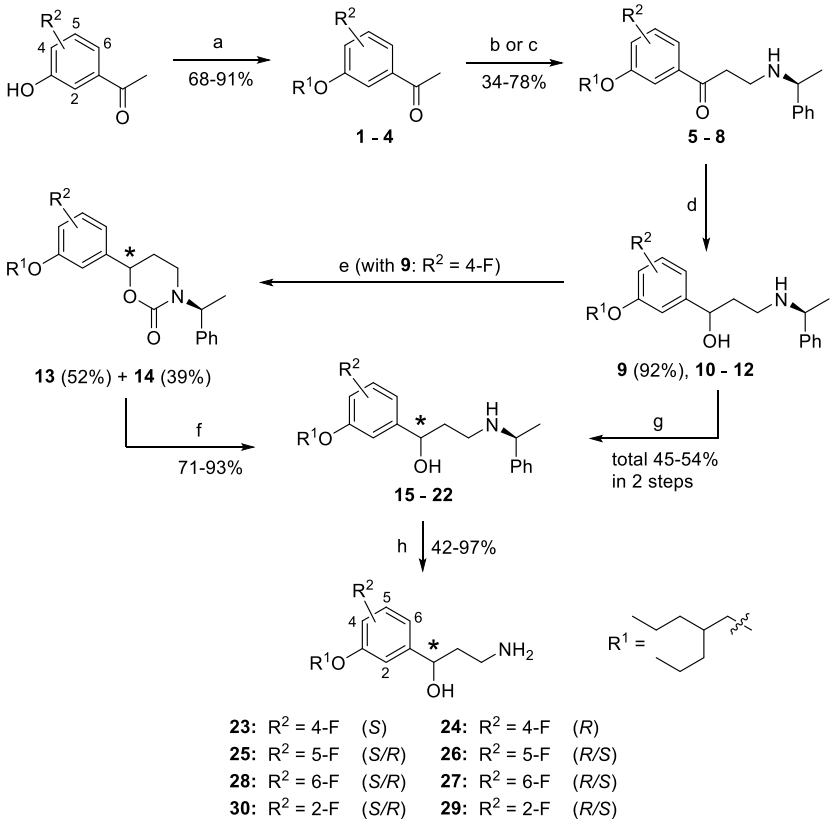

[a]Reagents and conditions: (a) 2-Propylpentyl mesylate, K_2CO_3, and DMF, 85 °C, 2−4 h. (b) Paraform, (*S*)-(−)-methylbenzylamine, conc. HCl (cat.), and 1,4-dioxane, MW, 100−130 °C, 5 min and (c) 1,3,5-trioxane, (*S*)-(−)-methylbenzylamine, conc. HCl (cat.), and 1,4-dioxane, sealed tube, 110 °C, overnight. (d) $NaBH_4$ and MeOH, r.t., 1 h. (e,i) CDI and THF, reflux, overnight; (ii) separation of diastereomers by FC on SiO_2. (f) KOH and EtOH, reflux, overnight. (g) Separation of diastereomeric mixtures **10**−**12** by chiral HPLC. (h) Ammonium formate, Pd/C (cat.), and MeOH, reflux, 30 min.

Scheme 2. Synthesis of Racemic Fluorinated Emixustat Analogues 49−59 via the Addition of Acetonitrile to Functionalized Benzaldehydes[a]

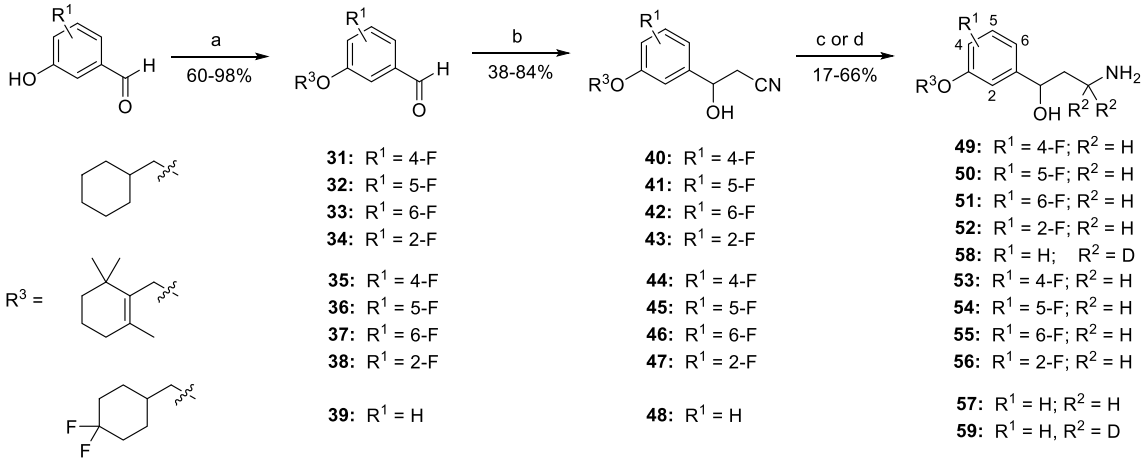

[a]Reagents and conditions: (a) R^3-Br or R^3-OMs, K_2CO_3, and DMF, 80−90 °C, overnight. (b) MeCN, *t*-BuOK, and THF, −50 °C, or LDA and THF, −78 °C; 1.5−3.0 h. (c) LAH and THF, 0 °C, 0.5−1.0 h. (d) LAD and THF, 0 °C, 1 h.

separated to single diastereomers **15**−**22** using preparative chiral high-performance liquid chromatography (HPLC) as detailed in the Supporting Information. The final N-deprotection of individual diastereomers **15**−**22** through Pd/C-catalyzed transfer hydrogenation with ammonium formate as a hydrogen source afforded the target γ-hydroxyalkylamines **23**−**30** as single enantiomers, which were studied biologically without further characterization of absolute stereochemistry. For a more detailed biological evaluation, the most active chiral 3-alkyloxy-4-fluoro derivative **24** as well as its enantiomer **23**

https://doi.org/10.1021/acs.jmedchem.1c00279
J. Med. Chem. 2021, 64, 8287−8302

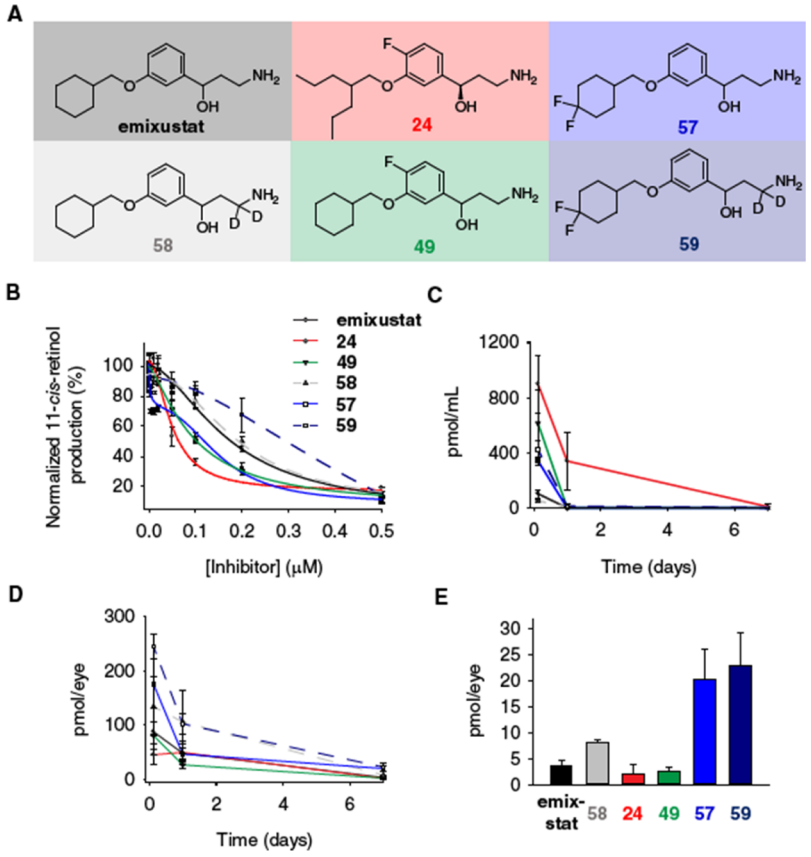

Figure 2. (A) Structures of visual cycle modulators used for pharmacokinetic studies. (B) Evaluation of the inhibitory effects of selected visual cycle modulators on 11-*cis*-retinol production by bovine RPE microsomes. Data points are shown as mean ± s.d.; $n = 3$. (C,D) Progress of visual cycle modulator elimination in the mouse serum (C) and eyes (D) after a single dose of intraperitoneal injection. Data points are shown as mean ± s.d.; $n = 4–5$. (E) Primary amine levels in mouse eyes on day 7 after the treatments.

Table 1. Mannich-Derived γ-Hydroxyamines

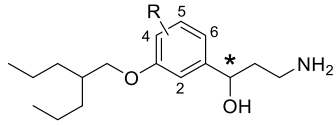

compound	*	*R*	IC_{50} (nM)	compound	*	*R*	IC_{50} (nM)
24	*R*	4-F	50 ± 9	**23**	*S*	4-F	177 ± 11
25	*R/S*	5-F	295 ± 132	**26**	*R/S*	5-F	184 ± 24
28	*R/S*	6-F	132 ± 19	**27**	*R/S*	6-F	157 ± 24
30	*R/S*	2-F	274 ± 47	**29**	*R/S*	2-F	287 ± 28

were synthesized by a more practical method, avoiding laborious and time-consuming preparative HPLC separation. Thus, a mixture of diastereomeric *N*-benzylated γ-amino-alcohols **9** was treated with 1,1′-carbonyldiimidazole (CDI)[29] giving almost quantitatively a mixture of chiral diastereomeric cyclic carbamates, which was readily separated to single components **13** (52%) and **14** (39%) by routine flash chromatography (FC) on silica gel. The cyclic carbamates **13** and **14** were separately hydrolyzed with KOH,[30] thus resolving acyclic *N*-benzylated γ-aminoalcohols **15** (93%) and **16** (71%). The γ-aminoalcohols **15** and **16** were N-deprotected as above (ammonium formate in MeOH, Pd/C-catalyst) giving the corresponding enantiomeric γ-aminoalcohols **23** (91%) and **24** (93%). A comparison of the duplicated specific rotation values $[\alpha]_D^{25}$ −21.32° (c = 0.0003, CH_2Cl_2) in **23** and +21.56° (c = 0.0002, CH_2Cl_2) in **24** with the reported data $[\alpha]_D^{26.7}$ + 19.66 (c = 0.01125, EtOH) for (*R*)-emixustat[31] tentatively favor the assignment of the absolute *R*-configuration for **24** and the opposite *S*-configuration for **23**. However, for a better understanding of the SAR additional structural study of the chiral γ-aminoalcohols **23**–**30** would be desirable.

The synthesis of the racemic fluorinated emixustat analogues **49**–**59** was performed through an alternative three-step synthetic route (Scheme 2) similar to the method elaborated for the parent emixustat.[5,19,31−33] After the alkylation of fluorinated hydroxybenzaldehydes to give the alkoxy derivatives **31**–**39**, treatment of the latter with deprotonated acetonitrile led to a three-atom elongation with the formation of the corresponding β-hydroxy-β-arylpropionitriles **40**–**48** (38–84%). The nitrile groups in these advanced intermediates **40**–**48** were either reduced with LAH to give racemic γ-aminoalcohols **49**–**57** or reduced and α-*bis*-deuterated with

https://doi.org/10.1021/acs.jmedchem.1c00279
J. Med. Chem. 2021, 64, 8287−8302

Table 2. α-Cyano Alcohol-Derived γ-Hydroxyamines

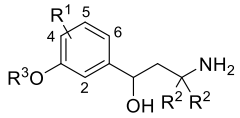

Compound	R3	R1	R2	IC50 (nM)	Compound	R3	R1	R2	IC50 (nM)
Racemic emixustat		H	H	172 ± 29	**(R)-MB-001**		H	H	323 ± 145
49		4-F	H	95 ± 5	**53**		4-F	H	284 ± 20
50		5-F	H	201 ± 23	**54**		5-F	H	292 ± 89
51		6-F	H	145 ± 9	**55**		6-F	H	124 ± 21
52		2-F	H	358 ± 42	**56**		2-F	H	169 ± 13
58		H	D	190 ± 15	**57**		H	H	103 ± 29
					59		H	D	269 ± 40

lithium aluminum deuteride (LAD) to give the *bis*-deuterio analogues **58** and **59** in variable yields. Although β-hydroxypropionitriles **40**−**48** might be potentially converted to an enatioenriched or enantiopure state using an additional oxidation/asymmetric reduction sequence as described for emixustat,[31,34] in this study the fluorinated emixustat analogues **49**−**59** were preliminary evaluated in the racemic form, as mixtures of their (*S*)- and (*R*)-enantiomers.

Inhibitory Properties and Pharmacokinetics of the Tested Compounds. A total of 19 novel emixustat derivatives were synthesized, and their inhibitory effects on RPE65 *in vitro* were characterized by the decrease of 11-*cis*-retinol production by bovine RPE microsomes (Figure 2A,B, Table 1, Supporting Information Table S1).[5] All of the synthesized primary amines showed an intense inhibitory activity toward RPE65 at submicromolar concentrations. Compared to emixustat and MB-001, a single fluorination at C4 of the phenyl ring significantly increases the inhibitory potency. Pronounced enhancement is seen with compound **24** (IC_{50} = 50 ± 9 nM), the most potent RPE65 inhibitor that we have identified to date, with an inhibitory potency 3 times greater than that of the racemic emixustat (IC_{50} = 172 ± 29 nM) and twice that of (*R*)-MB-004 (IC_{50} = 106 ± 16 nM),[33] which is the parent molecule of compound **24** lacking the 4-fluorine substitution. The *gem*-difluorination of the cyclohexyl ring in **57** also enhanced the inhibition of 11-*cis*-retinol production. The inhibition curve of **57** was found to exhibit a double sigmoidal feature indicative of two distinct modes of inhibitor binding to RPE65 (Table 2).

Oxidative deamination and hydroxylation on the cyclohexyl ring are two pathways for emixustat elimination *in vivo*;[17] the former being more dominant in the vasculature as compared to the liver.[17] By analogy to the studies of oxidative deamination of other compounds,[35] deuteration at the position α to the amino group of emixustat would be predicted to slow down its metabolic elimination due to a primary kinetic isotope effect. We explored this possibility by comparing the rate of oxidative deamination of emixustat and its α-deuterated derivative of emixustat (compound **58**) in an HPLC-based activity assay using mouse aorta homogenates as the source of the vascular adhesion protein-1 (VAP-1) enzyme (Figure 3A). We monitored the formation of the dehydrated aldehyde product of VAP-1 catalysis (**ACU-5201**) by reverse-phase HPLC (Figure 3B) whose identity and absolute amount were determined by comparison to an authentic synthetic standard (Figure 3B,C). As compared to emixustat, the formation of ACU-5201 from compound **58** was reduced by approximately 66% at both time points examined (Figure 3D). These data are consistent with the idea that proton abstraction from amine α-carbon is a rate-limiting step in the catalytic mechanism of emixustat deamination by VAP-1.

To investigate the impact of fluorination and deuteration on the elimination of emixustat in mouse eyes, a single dose of 380 nmol of emixustat, **24**, **49**, **57**, **58**, or **59** was individually administered to wild-type mice by intraperitoneal injection. The concentrations of the administered compounds found in mouse eyes were quantified by a mass spectrometry (MS) method (Figure 2A,D,E).[19] Most compounds were monitored for the loss of water (−18 Da) in the liquid chromatography

https://doi.org/10.1021/acs.jmedchem.1c00279
J. Med. Chem. 2021, 64, 8287−8302

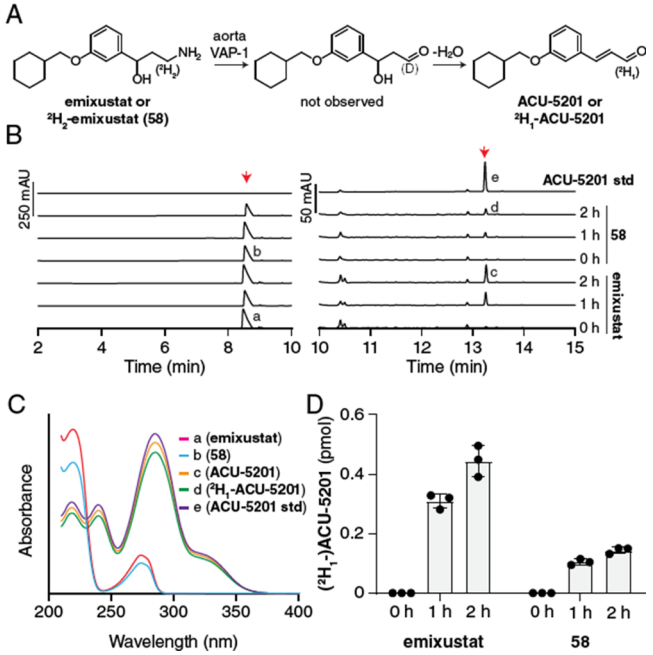

Figure 3. Impact of emixustat deuteration on VAP-1 metabolic susceptibility. (A) Scheme showing the oxidation of emixustat or **58** (^{2}H-emixustat) by VAP-1 present in the aorta homogenates used for the assay. (B) HPLC chromatographs showing the formation of ACU-5201 (right red arrow) over time, after incubation of emixustat or **58** (left red arrow) with mouse aorta homogenates containing VAP-1. The HPLC traces are split at 10 min with two different scales used to aid in visualization. (C) Identities of the product peaks verified by comparison of their retention times and UV/vis absorbance spectra to that of the authentic ACU-5201 standard. (D) Quantification of product formation showing that the deuteration at the 3-position reduced product formation nearly 3-fold at both 1 and 2 h time points. Mean values ± SDs and individual data points are shown in the graph.

(LC)−MS/MS−electrospray ionization (ESI) fragmentation spectra. An exception was **58**, in which the loss of water plus methylene imine (−47 Da) was monitored due to a high background effect of the fragmentation at −18 Da.

We first measured the total plasma concentrations of these compounds at 3 h, 1 d, or 7 d after compound administration (Figure 2C). Interestingly, we observed that compounds **24** and **49**, which both contain 4-fluoro substituents, exhibited the highest initial plasma levels suggesting that this modification can deactivate elimination pathway(s) of relevance in mice. Unexpectedly, we observed that $^2H_2$ emixustat had an initial serum concentration comparable to that of emixustat, which suggests that VAP-1 may not be a major pathway of emixustat clearance in the mouse. 1 d after injection, all compounds beside **24** were below the limits of detection. The longer plasma half-life of compound **24** is likely due to its more flexible alkyl substituents, which may be less susceptible to oxidation.

Next, we measured the distribution and retention of these compounds into the mouse eye. Emixustat was efficiently distributed to the ocular tissue reaching 88 ± 43 pmol/eye at 3 h after i.p. drug administration, nearly equal to 15% of the rhodopsin content in mouse eyes. 5″-*gem*-Difluorination of emixustat cyclohexyl (i.e., compound **57**) further enhanced ocular distribution. Compound **57** reached a concentration of 176 ± 93 pmol/eye, almost twice that of emixustat at the same time after administration. Interestingly, we observed that compounds **24** and **49**, which displayed the highest initial plasma concentrations, exhibited the poorest distribution within the ocular tissue. These data point to a possible ocular uptake mechanism for emixustat that is disrupted by 4-fluorination. Scrutiny of the mass spectra for **24** and **59** standards revealed that their peak intensities in methanol were much weaker than (about 5−10%) the peak intensities of emixustat and **57** standards in methanol at the same concentration. In the tandem mass spectra, **24** and **49** were also resistant to losing the methylene imine fragment. The difficulty of ionization and fragmentation of **24** and **49** in MS implies that 4-fluorination on the phenyl ring might intensify the intramolecular N−H−O hydrogen bonding interaction and reduce the molecular flexibility to hamper drug delivery to the eye. In our previous studies, most drug candidates against light-induced retinal degeneration decayed to negligible levels just 24 h after a single-dose intraperitoneal injection.[36] By contrast, emixustat and most of its fluorinated derivatives only moderately declined to around 50 pmol/eye during the same period, approximating 10% of the rhodopsin content. On day 7, the level of emixustat further dropped to about 4 pmol/eye, which is too low for all-*trans*-retinal sequestration but still sufficient to inhibit RPE65 activity and visual chromophore recovery.[19]

The level of deuterated emixustat, **58**, in the eye was approximately twofold higher than that of emixustat. In light of the plasma level data presented above, we cannot attribute this elevation to high circulating concentrations favoring distribution into the ocular tissue. Instead, it is possible that deuteration could positively impact ocular drug retention or affect metabolism within the eye by as-yet undefined processes. On the other hand, compound **57**, in which hydroxylation was partially blocked due to the *gem*-difluoro substitution on the C-5″ position, was found at a concentration of 21 ± 5.7 pmol in mouse eyes even after 7 days of a single intraperitoneal injection (Figure 2D,E). This amount is 5 times higher than that for emixustat and 10 times higher than that of compounds **24** and **49**; and it is an effective amount for the sequestration of excessive all-*trans*-retinal.[36] These results suggest that compound **57** is a promising next generation visual cycle modulator against retinal degeneration due to its higher inhibition potency, more specific delivery, and slower decay in the eye.

Crystal Structures of RPE65 in Complex with Fluorinated Visual Cycle Modulators. To gain an understanding of the factors underlying the enhanced potency of compounds **24**, **49**, and **57** compared to their parent molecules, we determined the crystal structures of RPE65 in complex with each of these compounds. The crystals were isomorphous to prior RPE65 structures in space group $P6_5$ and diffracted X-rays to resolutions of 1.95, 2.15, and 1.90 Å, respectively (Supporting Information Table S2). The structures were refined to overall R_{free} values of 21.1, 21.7, and 20.1% with excellent geometrical and clash score statistics (Supporting Information Table S2). A 2.1 Å resolution structure of apo-RPE65 was also determined for comparison (Supporting Information Table S2). Unbiased residual maps obtained after the first rounds of refinement in the absence of modeled ligands revealed a clear $|F_o|-|F_c|$ density for the bound visual cycle modulators in the proximal active site region, including well-defined features corresponding to the fluoro substituents (Figure 4). Residual electron density was

https://doi.org/10.1021/acs.jmedchem.1c00279
J. Med. Chem. 2021, 64, 8287−8302

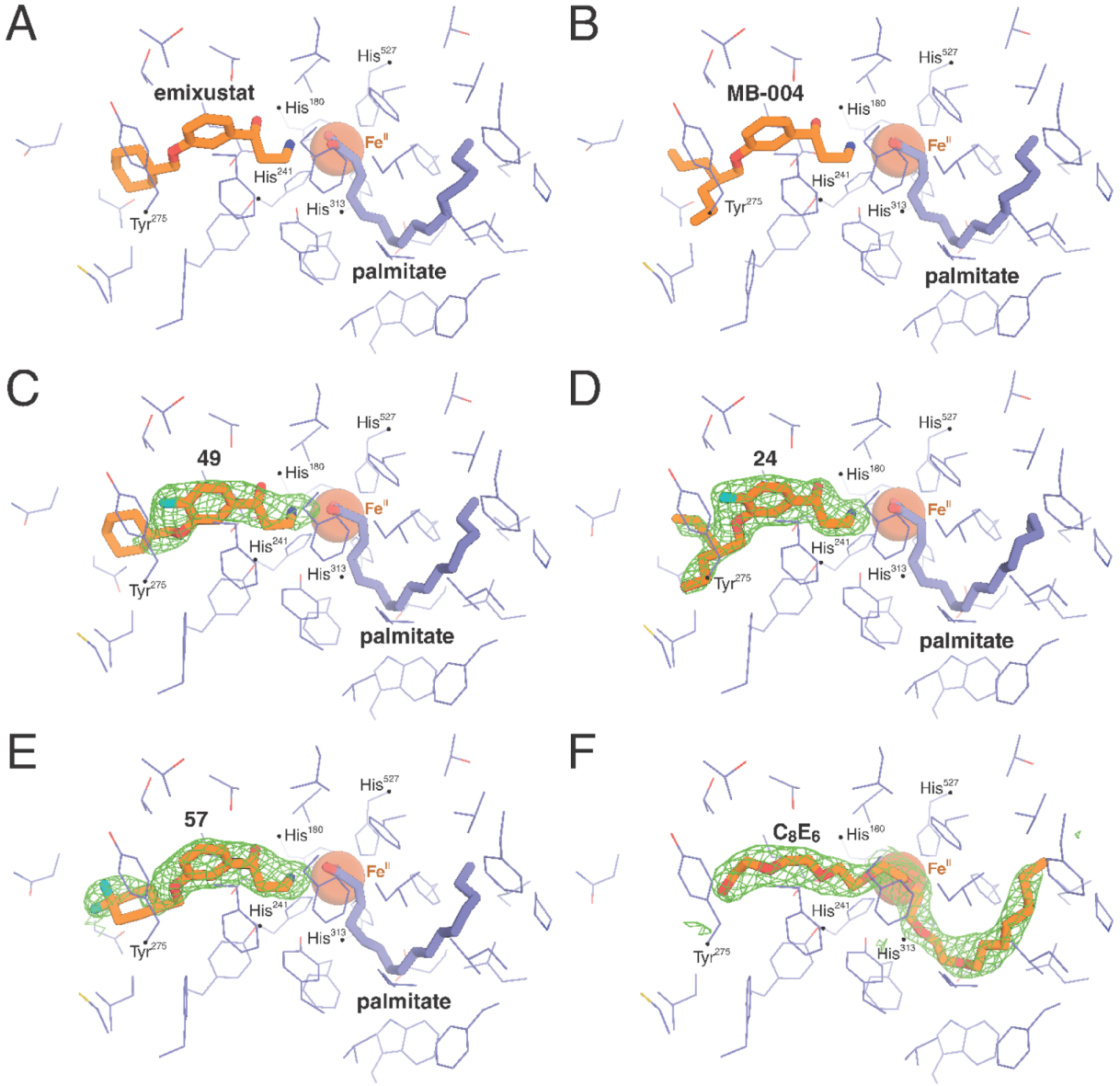

Figure 4. Crystal structures of bovine RPE65 in complex with (A) emixustat (PDB accession code 4RSC),[32] (B) MB-004 (PDB accession code 5ULS[33]), (C) C-4-fluoro-emixustat (compound **49**), (D) C-4-fluoro-MB-004 (compound **24**), (E) C-4-difluoro-emixustat (compound **57**), and (F) detergent hexaoxyethylene monooctyl ethyl (C_8E_6). The green mesh represents unbiased sigma-A weighted $|F_o|-|F_c|$ electron density contoured at 3 rmsd calculated prior to modeling the ligand.

also present in the distal cavity corresponding to a palmitate molecule forming a coordinate bond with the iron prosthetic group via its carboxylate moiety, consistent with prior findings.[32,33] Electron density maps following the inclusion of the inhibitor ligand in the model showed a well-defined density for the aryl γ-hydroxypropylamine moiety in all cases. The β,β-dipropylethoxy group of **24** was similarly well defined, whereas the densities for the cyclohexylmethoxy groups of **49** and **57** were comparatively much weaker (Figure 4). The relative quality of the electron density support for these different moieties is consistent with prior studies on emixustat and MB-004.[32,33] The crystal structure of apo-RPE65 featured an active site $|F_o|-|F_c|$ density consistent with hexaethylene glycol monooctyl ether (C_8E_6).

Linear detergents are known to inhibit the activity of RPE65[37,38] and related carotenoid oxygenase enzymes.[39,40] The structure of RPE65 solved with C_8E_6 bound to its active site provides evidence that such inhibition can be partially attributed to direct active site binding.[37] Despite the high concentration of the detergent in the crystallization mother liquor (>16 mM), compounds **24**, **49**, and **57** were able to outcompete the detergent for binding to the RPE65 active site, consistent with their strong active site-binding affinities.

The binding modes for compounds **24**, **49**, and **57** largely overlap with those of MB-004 and emixustat with a few notable exceptions (Figure 4). The binding mode of the aryl γ-hydroxypropylamine moiety of compound **57** was similar to that of emixustat (Figure 4A,E), whereas its terminal ring was rotated by ~90° as evidenced by clear electron density for its *gem*-difluoro moiety. This change in the cyclohexyl ring position was likely driven by fluorine-associated steric effects. Notably, a similar ring positioning was observed previously for emixustat in a $P6_522$ RPE65 crystal form (PDB accession code 4RYX). In this position, the *gem*-difluoro moiety engages in

https://doi.org/10.1021/acs.jmedchem.1c00279
J. Med. Chem. 2021, 64, 8287−8302

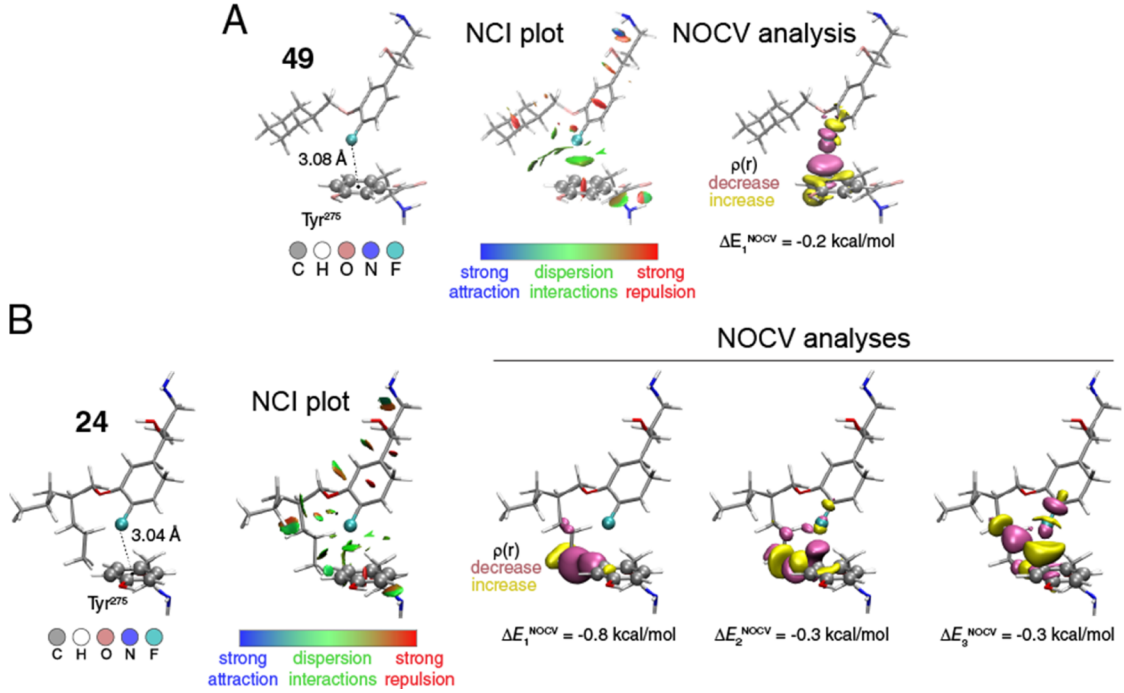

Figure 5. Theoretical analyses of the interactions of compound **49** (A) and compound **24** (B) with Tyr^{275}, using a model dimer system.

only a single van der Waals interaction with the Asn^{194} side chain oxygen atom. Although the bi-phasic IC_{50} curve for **57** suggested two modes of RPE65 binding (Supporting Information Table S1), we could not discern such behavior from the structural data, although it is notable that RPE65 is more poorly ordered near the active site opening in the structure of the RPE65 compound **57** complex as compared to the emixustat-bound structure. It is thus possible that multiple conformations, one of which has a higher affinity for **57**, could be responsible for the bi-phasic inhibition results. In the case of **49**, the C1″-O-C3-C2 dihedral angle is rotated by ∼49° compared to the corresponding angle in emixustat, which is nearly planar. The analogous dihedral angle in **24** similarly deviates from the planarity seen in MB-004 by ∼31°. These differences can be attributed to the presence of the nearby 4-fluoro group giving rise to two effects. First, the presence of the fluorine causes a ∼0.4 Å downward shift in the binding position of the aryl ring, which may necessitate a corresponding rotation in the C3″-O bond to avoid steric clashes with the oxy-linked alkane moieties. Second, the rotation could also be driven by electrostatic effects between the electron-dense fluoro moiety and the lone-pair electrons on the O atom of the aryl ether. In addition, the structure of the enzyme compound **24** complex revealed a conformational difference in one of the propyl groups of **24** as compared to the complex with MB-004.

The enzyme environment around the 4-fluoro substituent of the bound modulator is likely an important factor that could help explain the greater potency of the 4-fluoro compounds **24** and **49** compared to their parent molecules. The dominant interaction occurs with Tyr^{275} where the fluoro group makes a close (∼3−3.1 Å) en face contact with the aromatic ring. Compared to structures with the parent molecules bound, the Tyr^{275} side chain is rotated by ∼8° around the Cβ-Cγ bond, likely to alleviate steric clashes with the fluoro moiety or to facilitate the en face interaction. Redmond's lab has mutagenized position Tyr275 previously.[41] Only the aromatic residue Phe was partly active (44%), whereas other substitutions were inactive.

Quantum Chemical Analysis of the Aromatic−Fluoro Interaction Observed in Crystals. To further elucidate the energetics of the aromatic−fluoro interaction observed in the crystal structures, we employed quantum chemical calculations. One would expect the ∼3 Å interaction to be repulsive in the first approximation, as a highly electronegative F atom is brought in the close vicinity of an electron-rich π cloud. However, analogous stabilizing Cl−π dispersion-driven interactions are known in protein chemistry.[42] Their strength is on the order of 2 kcal/mol and are thought to be dispersion-driven forces. In contrast, F−π contacts have not been investigated thoroughly. Experiments based on synthetic models provide estimates of the stabilizing interaction of roughly 1.6 kcal/mol.[43] In recent work, Li and co-workers[44] found that the stability of the F−π interaction increases with positive charge accumulation in the π-system. Thus, the interaction seems to be mostly electrostatically driven.

Using dimer model systems obtained from the crystal structures (Figure 5), we estimated the strength of the interaction (ΔE_{int}) between Tyr^{275} and each of the two fluorinated compounds **49** and **24** to be −2.34 and −2.69 kcal/mol, respectively, using the state-of-the-art DLPNO-CCSD(T) method at the basis set limit.[45,46] The interaction energy was broken down into various contributions using the local energy decomposition (LED) scheme.[47] According to Table 3, the overall electrostatic interaction has a repulsive characteristic [$\Delta E_{HF\text{-}CCSD}$(electro) > 0]. Here, key stabilizing factors within this contribution are the electrostatic attraction between the "prepared" wavefunctions of the fragments ΔE_{HF}(elstat) and charge-transfer contributions ΔE_{CCSD}(CT). Both are significantly more negative for compound **24**. Within the latter, **24** → Tyr double excitations have a significant contribution (−3.70 kcal/mol). The overall repulsive electrostatic effects are compensated by the dispersion interactions ΔE_{CCSD}(disp) of −4.28 and −8.23 kcal/mol for compounds **49**

https://doi.org/10.1021/acs.jmedchem.1c00279
J. Med. Chem. 2021, 64, 8287−8302

Table 3. LED Analysis of the DLPNO-CCSD(T) Total Interaction Energy (ΔE_{int}) in the Crystal Structure-Derived Dimers of Compounds 49 and 24 with Tyr^{275}[a]

ΔE [kcal/mol]	49	24
$\Delta E_{HF\text{-}CCSD}$(electro) including	1.87	5.80
ΔE_{HF}(el-prep)	8.46	27.11
ΔE_{CCSD}(el-prep)	1.51	5.33
ΔE_{HF}(elstat)	−4.77	−15.21
ΔE_{HF}(exch)	−1.58	−5.71
ΔE_{CCSD}(CT EmixF → Tyr)	−1.58	−3.70
ΔE_{CCSD}(CT Tyr → EmixF)	−0.17	−2.02
ΔE_{CCSD}(disp)	−4.28	−8.23
$\Delta E(T)$	−0.47	−1.10
ΔE(CBS)	0.54	1.01
ΔE_{int}	−2.34	−2.69

[a]All values are in kcal/mol.

and **24**, respectively. The magnitude of ΔE_{HF}(elstat) and ΔE_{CCSD}(disp) is similar; thus, one can say that both electrostatic and van der Waals forces are driving the examined interactions.

To further investigate the nature of the interaction between Tyr^{275} and compounds **49** and **24** in 3D space, we performed a noncovalent interaction (NCI) analysis (Figure 5).[48] Briefly, the NCI plot shows low-density and low-gradient regions that are associated with NCIs, colored according to one of the components of the density Laplacian (λ_2): strong attractive interactions appear at $\lambda_2 < 0$ (e.g., H-bonds; blue in Figure 5), while steric repulsion is associated with positive values of λ_2 (red in Figure 5). Dispersion forces appear with small negative values around $\lambda_2 \approx 0$ (green in Figure 5). The examined systems' NCI plots revealed a significant dispersion interaction region in the middle between the F atom of both **24** and **49** and the π-plane of Tyr^{275} (Figure 5: isovalue of $s = 0.6$ a.u., colored according to $-0.035 < \text{sign}(\lambda_2)\rho < 0.02$). Another way to look at intermolecular interactions is to study natural orbitals for chemical valence (NOCV)[49] within the density functional theory (here, we used the ωB97X-D3BJ functional).[50,51] Briefly, we start by considering isolated fragments 1 and 2 at the geometry of a dimer. The two are characterized with the electron densities ρ_1 and ρ_2, respectively. A simple union of these densities yields pro-molecular density $\rho^{pro} = \rho_1 + \rho_2$ along with an associated pro-molecular wave function Ψ^{pro}. Self-consistent optimization of the latter provides Ψ^{opt} with the optimal density ρ^{opt}. We then define deformation density $\Delta\rho$ as the difference between pro-molecular density and self-consistently converged density $\Delta\rho = \rho^{pro} - \rho^{opt}$. Eigenorbitals of the corresponding deformation density operators are called NOCVs, and typical bonding and antibonding pairs are described with complementary NOCVs ($\varphi_{\pm n}$).

With each such pair, we associate the orbital deformation density $\Delta\rho_n^{orb}$

$$\Delta\rho_n^{orb} = -\nu(\varphi_{-n})^2 + \nu(\varphi_n)^2$$

where ν is the corresponding NOCV eigenvalue. By using the extended transition state theory (ETS),[52] one assigns a particular energy portion to such orbital interaction. By summing up all NOCV interaction energies, one obtains the so-called orbital-interaction energy. In the case of our dimers, this yields −0.7 and −2.4 kcal/mol for **49** and **24**, respectively. The orbital-interaction energies should be attributed mainly to electrostatic stabilization of the electron density in the dimers and less to dispersion. The latter is added a posteriori in our calculations, and it does not influence the density distribution directly—the total interaction energy (including dispersion correction) is −2.3 kcal/mol for **49** and −3.4 kcal/mol for **24**. In this context, up to three significant NOCV complementary pairs yield deformation densities, as shown in Figure 5 (±0.005 a.u. isosurface), that account for up to 60% of the orbital interaction energies in both cases. In the case of **24**, the key ingredients are the interactions between the *n*-propyl chain and the Tyr^{275} phenyl ring ($\Delta\rho_1^{orb}$, $\Delta\rho_2^{orb}$). The inspection of $\Delta\rho_3^{orb}$ shows that the region between the F atom and phenyl ring gains some electron density. At the same time, electron density reorganization takes place at both fragments within σ(C−F)/σ^*(C−F)/n(F) and π(phenyl)/π^*(phenyl) orbitals of **24** and Tyr^{275}, respectively. The electron density reorganization for **49** compared to **24** is less pronounced and is reflected in the overall diminished interaction energy.

DISCUSSION AND CONCLUSIONS

Emixustat, a first-in-class visual cycle modulation drug candidate has displayed promising *in vitro* and *in vivo* properties for the treatment of a variety of retinal diseases. However, emixustat suffers from sub-optimal efficacy, problematic side effects, and rapid metabolism, which cloud its clinical future.[17]

This work investigates whether fluorination and/or deuteration of emixustat can eliminate the pharmacokinetic shortcomings of this clinical candidate. We developed novel synthetic approaches to produce specific chiral products as emixustat's inhibitory activity toward RPE65 was previously shown to depend on the C1 stereochemistry.[19] We present an advanced three-component Mannich reaction utilizing (*S*)-(−)-α-methylbenzylamine to produce the desired stereoisomer. In this reaction scheme, the resultant from the subsequent reduction step, γ-hydroxypropylaminobenzyl product(s), consists of a mixture of diastereomers that can be carbamylated and separated using conventional flash column chromatography on silica gel as opposed to chiral chromatography required for the separation of the parent enantiomers. Facile hydrolysis of the carbamate succeeded by debenzylation regenerates the key γ-hydroxypropylamine framework with the defined stereochemistry. This method provides clear advantages in terms of cost and scalability over chiral separation methods and perhaps can extend to other similar compounds.

We investigated the impact of these emixustat and emixustat-derived compounds **57**, **58**, and **59** on RPE65 activity *in vitro* and in live mice. Our first observation was that RPE65 inhibition does not correlate with accumulation in the eye. **57**, **58**, and **59** accumulate more in the eye than emixustat, as shown in Figure 2, possibly due to an increase in metabolic stability or selective uptake or retention by an as-yet undefined ocular component. The half-lives of the *gem*-difluoro molecules, **57** and **59**, are higher than that of **58**, which is at least in part due to the greater metabolic stability from the abrogation of known oxidation pathways of the cyclohexyl moiety, and it is possible that other factors are at play. Another possible explanation for this prolonged half-life effect is that the *gem*-difluoro molecules could be transported to or retained within ocular tissues (e.g., by promoting melanin binding) more efficiently than their non-fluorinated counterparts. Practically, **57** or *gem*-difluoro-emixustat has better pharmaco-

https://doi.org/10.1021/acs.jmedchem.1c00279
J. Med. Chem. 2021, 64, 8287−8302

kinetic properties than emixustat in terms of elimination half-life and consequent swings in eye levels, solving some of the problems associated with the use of emixustat in humans.

VAP-1 is a lesser known phase-1 metabolic pathway[53] important for the primary amine oxidation of clinically used drugs including primaquine[54] and tresperimus[55] in addition to emixustat.[15] Our results here suggest that the deuteration of primary amines susceptible to VAP-1 oxidation could be a generally effective approach to prolonging their *in vivo* activity. The impact of alpha deuterium substitution of amines on VAP-1 metabolic susceptibility was previously studied *in vitro* using benzylamine and various phenylethylamines as test substrates.[56] A variety of para-substituted phenylethylamines, whose amine protons are in an environment similar to those of emixustat, all displayed kinetic isotope effects on k_{cat} of ∼5−8, which is within the theoretically expected primary kinetic isotope effect (i.e., KIE = 3−7),[57−60] for a reaction with a rate-limiting proton abstraction step. Our data showing impaired oxidation of deuterated emixustat as compared to emixustat are consistent with hydrogen abstraction being at least partially rate-limiting in the mechanism of emixustat oxidation by VAP-1.

The structure−activity relationships presented here are largely consistent with previous observations including higher inhibitory activity for the *R*-versus *S*-isomer of the γ-aminoalcohol (Table S1, compare **24** to **23**),[19] as well as for compounds with a β,β-dipropylethoxy substituent as opposed to a cyclohexyl or β-ionone moiety.[33] Our structural biology results support our previous findings that the β,β-dipropylethoxy group[19,33] can engage binding pockets within the RPE65 active site cavity that are not accessible to a cyclohexyl group, which likely improves the binding affinity of these compounds. We expand the known SAR of RPE65 inhibitors to include the effects of fluorine substitution throughout the base structures of emixustat, MB-001 and MB-004. We found that fluorine substitution on the aryl moiety could have either a positive or negative impact on inhibitory activity. A notable favorable impact was the 4-fluoro derivative of MB-004 (compound **24**) and 4-fluoro-emixustat (**49**), which exhibited an IC_{50} value (50 nM) approximately 2-fold lower than MB-004 and emixustat, respectively. Structurally, the enhanced affinity appears to result from an energetically favorable interaction between the fluoro substituent and an active site tyrosyl side chain (Tyr^{275}). According to our calculations, the key stabilization is provided by van der Waals[42] contributions as opposed to electrostatic interactions consistent with the electron-rich nature of the phenolic side chain. The introduction of a *gem*-difluoro group at the 5″ position of the cyclohexyl ring of emixustat (compound **57**) also strengthened the inhibitory activity, although the structural basis for this effect was less clear given that the *gem*-difluoro group interacts minimally with the RPE65 active site pocket. The *gem*-difluoro substitution is both pharmacokinetically and pharmacodynamically favorable and should be considered in the future development of other emixustat derivatives to improve *in vivo* activity.

EXPERIMENTAL SECTION

Chemistry. All reactions were performed in oven-dried glassware under a dry argon or nitrogen atmosphere. Synthesis under MW irradiation was performed with a Biotage, Initiator+ Robot Eight microwave system (Charlotte, NC). Lithium aluminum deuteride [98 atom% $^{2}H(D)$] was purchased from Millipore Sigma Isotopes (Miamisburg, OH). All other reagents were used as supplied without purification. Analytical thin-layer chromatography (TLC) was performed on 0.25 mm glass-backed EMD Millipore 60 F254 plates. Visualization of the developed chromatogram was accomplished with UV light (254 nm) and stained with either ethanolic phosphomolybdic acid, ceric ammonium molybdate, or permanganate ($KMnO_4$). LC was performed using a forced air-flow (FC) on silica gel (Merck, 230−400 mesh), using eluting solvents (reported as V/V ratio mixture). The ^{1}H, ^{13}C[61]/DEPT, ^{19}F NMR, and 2D-nuclear magnetic resonance (NMR) spectra were recorded at 25 °C on Bruker AVANCE NMR spectrometers operating at 300, 400, 500, 600, and 700 MHz for the ^{1}H channel and were in accordance with the assigned structures. ^{19}F NMR spectra were recorded without decoupling from protons. Chemical shifts were reported in δ units, part per million, with reference to the residual solvent peak $CDCl_3$ (δ 7.26), CD_3OD (δ 3.31), and C_6D_6 (δ 7.16) for ^{1}H and $CDCl_3$ (δ 77.36), CD_3OD (δ 49.00), and C_6D_6 (δ 128.06) for ^{13}C spectra or TMS (δ 0.00). NMR data are presented in the following order: chemical shift, peak multiplicity (b = broad, s = singlet, d = doublet, t = triplet, q = quartet, m = multiplet, dd = doublet of doublet, ddd = doublet of doublet of doublet, ddt = doublet of doublet of triplet, dq = doublet of quartet, dm = doublet of multiplet, and br = broad), coupling constant (in Hz). The specific light rotations were measured with a JASCO digital polarimeter (Model P-1010, λ = 589 nm, ±0.05° accuracy) using a cylindrical quartz cell (5 mL, *l* = 5 cm) at 25 °C. Mass spectra were recorded in positive ionization mode on an Agilent 6545 QTOF mass spectrometer (Agilent Technologies, USA), equipped with ESI and atmospheric pressure chemical ionization interfaces coupled to an Agilent 1260 ultrahigh-pressure LC (UHPLC) (Agilent Technologies, Santa Clara, CA, USA). The Agilent 1260 series system consists of a G4204A quaternary pump, a G4226A ALS auto-sampler, and a G1316C column compartment. UHPLC was carried out on a ZORBAX RRHD Eclipse Plus C18, 95 Å, 2.1 × 50 mm, 1.8 μm column (Agilent Technologies, USA) column with H_2O (0.1% formic acid)−acetonitrile gradient elution from 5 to 95% acetonitrile in the course of 10 min at a flow rate of 0.5 mL/min. Preparative and analytical HPLC were performed on a HPLC system (Young Lin Instruments, Anyang, Korea) with a LUNA C18(2) (10 μm, 250 mm × 21.2 mm) column and a chiral column LUX Amylose-1 (5 μm, 250 mm × 21.2 mm), for preparative purification, and (5 μm, 250 × 4.6 mm), for analysis, all from Phenomenex, Inc. (Torrance, CA). Acetonitrile and double-distilled water in different ratios were used as an eluent. The final biologically tested compounds displayed ≥95% purity (confirmed using analytical HPLC). Compound **57** was obtained at 90% purity. Synthesis of the final emixustat analogues is detailed herein, while the synthesis of all the precursors is described in the Supporting Information.

*(S)-3-Amino-1-(4-fluoro-3-((2-propylpentyl)oxy)phenyl)propan-1-ol (**23**). General Procedure.* The N-protected aminoalcohol **15** (280 mg, 0.70 mmol) was suspended with 10% Pd/C (100 mg) in dry MeOH (4 mL) under a nitrogen atmosphere. After 30 min, solid ammonium formate (1.29 mmol) was added. The resulting mixture was refluxed (TLC monitoring), cooled to 0 °C, filtered through a celite pad, and washed with chloroform. The filtrate was concentrated under reduced pressure to afford the corresponding title γ-aminoalcohol **23** (188 mg, 91%) as colorless oil. [α]D25 = −21.32° (*c* = 0.0003, CH_2Cl_2). ^{1}H NMR (300 MHz, $CDCl_3$): δ 7.23−6.85 (m, 2H), 6.80 (ddd, *J* = 2.0, 4.0, 8.0 Hz, 1H), 4.82 (dd, *J* = 3.0, 8.5 Hz, 1H), 3.89 (d, *J* = 5.5 Hz, 2H), 3.64 (bs, 2H), 3.37−2.96 (m, 1H), 2.96−2.59 (m, 1H), 2.07−1.57 (m, 3H), 1.56−1.19 (m, 8H), 0.91 (t, *J* = 7.0 Hz, 6H). ^{13}C NMR (75 MHz, $CDCl_3$): δ 151.7 (d, *J* = 244.5 Hz), 147.2 (d, *J* = 10.5 Hz), 141.4 (d, *J* = 3.5 Hz), 117.5 (d, *J* = 7.0 Hz), 115.5 (d, *J* = 18.5 Hz), 112.2, 74.3, 72.3, 40.1, 39.8, 37.6, 33.6, 19.9, 14.4. ^{19}F NMR (376 MHz, $CDCl_3$): δ −137.5 (m). HRMS (ESI): calcd for $C_{17}H_{28}FNO_2$ $[M + H]^+$, 298.2176; found, 298.2172.

*(R)-3-Amino-1-(4-fluoro-3-((2-propylpentyl)oxy)phenyl)propan-1-ol (**24**).* According to the general procedure, *N*-benzylated compound **16** (458 mg, 1.14 mmol) was deprotected to give the title γ-aminoalcohol **24** (314.2 mg, 93%) as colorless oil. [α]D25 = +21.56° (*c* = 0.0002, CH_2Cl_2). ^{1}H NMR (400 MHz, $CDCl_3$): δ 7.06−

https://doi.org/10.1021/acs.jmedchem.1c00279
J. Med. Chem. 2021, 64, 8287−8302

6.94 (m, 2H), 6.90−6.70 (m, 1H), 4.82 (dd, J = 3.0, 8.5 Hz, 1H), 3.89 (d, J = 5.5 Hz, 2H), 3.5 (bs, 2H), 3.20−3.02 (m, 1H), 3.00−2.90 (m, 1H), 1.89−1.80 (m, 2H), 1.78−1.68 (m, 1H), 1.49−1.20 (m, 8H), 0.91 (t, J = 7.0 Hz, 6H). ^{13}C NMR (100 MHz, $CDCl_3$): δ 151.8 (d, J = 244.5 Hz), 147.3 (d, J = 10.5 Hz), 141.2 (d, J = 3.5 Hz), 117.6 (d, J = 7.0 Hz), 115.6 (d, J = 18.5 Hz), 112.3, 74.7, 72.4, 40.2, 39.4, 37.6, 33.6, 19.9, 14.4. ^{19}F NMR (376 MHz, $CDCl_3$): δ −137.5 (m). HRMS (ESI): calcd for $C_{17}H_{28}FNO_2$ $[M + H]^+$, 298.2176; found, 298.2173.

*(R/S)-3-Amino-1-(3-fluoro-5-((2-propylpentyl)oxy)phenyl)-propan-1-ol (**25**).* According to the general procedure, *N*-benzylated compound **17** (236 mg, 0.59 mmol) was deprotected giving the chiral γ-aminoalcohol **25** (170 mg, 97%) as colorless oil. ^{1}H NMR (600 MHz, C_6D_6): δ 7.10−7.02 (m, 1H), 6.99−6.85 (m, 1H), 6.68−6.54 (m, 1H), 5.14−4.61 (m, 1H), 3.56 (d, J = 5.5 Hz, 2H), 2.50−2.35 (m, 1H), 2.34−2.14 (m, 1H), 1.70−1.62 (m, 1H), 1.49−1.19 (m, 10H), 0.87 (t, J = 7.0 Hz, 6H). ^{13}C NMR (150 MHz, C_6D_6): δ 164.3 (d, J = 244.0 Hz), 161.2 (d, J = 11.0 Hz), 150.0 (d, J = 8.5 Hz), 108.3 (d, J = 2.5 Hz), 105.0 (d, J = 22.0 Hz), 100.3 (d, J = 25.0 Hz), 75.1, 70.9, 40.7, 39.7, 37.8, 34.0, 20.3, 14.6. ^{19}F NMR (376 MHz, C_6D_6): δ −112.89 (t, J = 10.0 Hz). HRMS (ESI): calcd for $C_{17}H_{28}FNO_2$ $[M + H]^+$, 298.2176; found, 298.2179.

*(R/S)-3-Amino-1-(3-fluoro-5-((2-propylpentyl)oxy)phenyl)-propan-1-ol (**26**).* Deprotection of *N*-benzylated compound **18** (46 mg, 0.11 mmol) according to the general procedure afforded the chiral γ-aminoalcohol **26** (14.2 mg, 42%) as colorless oil. ^{1}H NMR (400 MHz, $CDCl_3$ + CD_3OD): δ 6.72−6.67 (m, 1H), 6.67−6.59 (m, 1H), 6.54−6.43 (m, 1H), 4.76 (dd, J = 4.0, 8.0 Hz, 1H), 3.80 (d, J = 5.5 Hz, 2H) 3.77 (bs, 2H), 3.07−2.70 (m, 2H), 1.86−1.73 (m, 3H), 1.50−1.24 (m, 8H), 0.91 (t, J = 7.0 Hz, 6H). ^{13}C NMR (100 MHz, $CDCl_3$ + CD_3OD): δ 162.7 (d, J = 244.0 Hz), 160.7 (d, J = 11.0 Hz), 148.25 (d, J = 8.5 Hz), 107.7 (d, J = 2.5 Hz), 104.5 (d, J = 22.0 Hz), 100.6 (d, J = 25.0 Hz), 73.1, 71.3, 40.0, 39.2, 37.5, 33.7, 20.0, 14.4. ^{19}F (376 MHz, $CDCl_3$ + CD_3OD): δ −112.74 (t, J = 10.0 Hz). HRMS (ESI): calcd for $C_{17}H_{28}FNO_2$ $[M + H]^+$, 298.2176; found, 298.2186.

*(R/S)-3-Amino-1-(2-fluoro-5-((2-propylpentyl)oxy)phenyl)-propan-1-ol (**27**).* According to the general procedure, *N*-benzylated compound **20** (30 mg, 0.07 mmol) was deprotected giving the chiral γ-aminoalcohol **27** (13.4 mg, 61%) as colorless oil. ^{1}H NMR (400 MHz, C_6D_6): δ 7.69 (ddd, J = 1.0, 3.0, 6.0 Hz, 1H), 6.83 (t, J = 9.5 Hz, 1H), 6.70−6.58 (m, 1H), 5.42 (dd, J = 1.0, 8.5 Hz, 1H), 3.70 (d, J = 5.5 Hz, 2H), 2.51−2.40 (m, 1H), 2.37−2.29 (m, 1H), 1.84−1.76 (m, 1H), 1.75−1.65 (m, 1H), 1.54−1.45 (m, 1H), 1.44−1.21 (m, 8H), 0.87 (t, J = 7.0 Hz, 6H). ^{13}C NMR (100 MHz, C_6D_6): δ 156.4, 154.2 (d, J = 236.0 Hz), 134.3 (d, J = 14.5 Hz), 115.6 (d, J = 23.5 Hz), 114.0 (d, J = 8.0 Hz), 113.4 (d, J = 4.5 Hz), 71.3, 70.1, 40.0, 38.6, 38.0, 34.1, 20.3, 14.6. ^{19}F NMR (376 MHz, C_6D_6): δ −131.25 (m). HRMS (ESI): calcd for $C_{17}H_{28}FNO_2$ $[M + H]^+$, 298.2176; found, 298.2178.

*(R/S)-3-Amino-1-(2-fluoro-5-((2-propylpentyl)oxy)phenyl)-propan-1-ol (**28**).* Following the general procedure, *N*-benzylated compound **19** (33 mg, 0.08 mmol) was deprotected giving the chiral γ-aminoalcohol **28** (15.2 mg, 61%) as colorless oil. ^{1}H NMR (700 MHz, C_6D_6): δ 7.71 (dd, J = 3.0, 6.0 Hz, 1H), 6.83 (t, J = 9.5 Hz, 1H), 6.71−6.56 (m, 1H), 5.43 (dd, J = 1.0, 8.5 Hz, 1H), 3.70 (d, J = 5.5 Hz, 2H), 2.52−2.37 (m, 1H), 2.37−2.29 (m, 1H), 1.85−1.75 (m, 1H), 1.75−1.63 (m, 1H), 1.51−1.43 (m, 1H), 1.43−1.20 (m, 8H), 0.86 (t, J = 7.0 Hz, 6H). ^{13}C NMR (176 MHz, C_6D_6): δ 156.3, 154.2 (d, J = 236.0 Hz), 134.3 (d, J = 14.5 Hz), 115.6 (d, J = 23.5 Hz), 114.0 (d, J = 8.0 Hz), 113.3 (d, J = 4.5 Hz), 71.3, 70.2, 41.0, 38.56, 38.01, 34.08, 20.35, 14.66. ^{19}F NMR (376 MHz, C_6D_6): δ −131.25 (m). HRMS (ESI): calcd for $C_{17}H_{28}FNO_2$ $[M + H]^+$, 298.2176; found, 298.2177.

*(R/S)-3-Amino-1-(2-fluoro-3-((2-propylpentyl)oxy)phenyl)-propan-1-ol (**29**).* According to the general procedure, *N*-benzylated compound **22** (36 mg, 0.09 mmol) was deprotected to give the chiral γ-aminoalcohol **29** (14.1 mg, 52%) as colorless oil. ^{1}H NMR (700 MHz, C_6D_6): δ 7.60 (t, J = 8.0 Hz, 1H), 7.07 (t, J = 8.0 Hz, 1H), 6.68 (dd, J = 1.0, 8.0 Hz, 1H), 5.44 (dd, J = 2.0, 8.5 Hz, 1H), 3.68 (dd, J = 2.0, 5.5 Hz, 2H), 2.45−2.39 (m, 1H), 2.33−2.29 (m, 1H), 1.80−1.70 (m, 2H), 1.55−1.47 (m, 1H) 1.46−1.23 (m, 8H), 0.88 (t, J = 7.0 Hz, 6H). ^{13}C NMR (176 MHz, C_6D_6): δ 150.0 (d, J = 244.5 Hz), 147.6 (d, J = 11.0 Hz), 134.6 (d, J = 10.5 Hz), 123.9 (d, J = 4.0 Hz), 119.3 (d, J = 3.5 Hz), 113.2, 72.2, 69.8 (d, J = 2.5 Hz), 40.8, 38.5, 38.0, 34.0, 20.3, 14.6. ^{19}F NMR (376 MHz, C_6D_6): δ −142.05 (t, J = 7.0 Hz). HRMS (ESI): calcd for $C_{17}H_{28}FNO_2$ $[M + H]^+$, 298.2176; found, 298.2187.

*(R/S)-3-Amino-1-(2-fluoro-3-((2-propylpentyl)oxy)phenyl)-propan-1-ol (**30**).* Following the general procedure, *N*-benzylated compound **21** (35 mg, 0.09 mmol) was deprotected giving the chiral γ-aminoalcohol **30** (13.6 mg, 52%) as colorless oil. ^{1}H NMR (400 MHz, C_6D_6): δ 7.60 (t, J = 1.0, 8.0 Hz, 1H), 7.01 (t, J = 8.0 Hz, 1H), 6.69 (t, J = 8.0 Hz, 1H), 5.44 (dd, J = 2.0, 8.5 Hz, 1H), 3.68 (d, J = 5.5 Hz, 2H), 2.40−2.38 (m, 1H), 2.34−2.27 (m, 1H), 1.82−1.69 (m, 2H), 1.54−1.48 (m, 1H) 1.46−1.21 (m, 8H), 0.88 (t, J = 7.0 Hz, 6H). ^{13}C NMR (100 MHz, C_6D_6): δ 150.12 (d, J = 244.5 Hz), 147.6 (d, J = 11.0 Hz), 134.6 (d, J = 10.5 Hz), 123.9 (d, J = 4.0 Hz), 119.3 (d, J = 3.5 Hz), 113.2, 72.2, 69.8 (d, J = 2.5 Hz), 40.8, 38.6, 38.0, 34.0, 20.3, 14.6. ^{19}F (376 MHz, C_6D_6): δ −142.11 (t, J = 7.0 Hz). HRMS (ESI): calcd for $C_{17}H_{28}FNO_2$ $[M + H]^+$, 298.2176; found, 298.2178.

*3-Amino-1-(3-(cyclohexylmethoxy)-4-fluorophenyl)propan-1-ol (**49**). General Procedure.* To a solution of compound **40** (8 g, 28.8 mmol, 1 equiv) in dry tetrahydrofuran (THF) (55 mL) was added lithium aluminum hydride (2.46 g, 64.9 mmol, 2.25 equiv) in portions under nitrogen at 0 °C, and then the reaction mixture was stirred at 0 °C for another 0.5 h. The reaction was quenched with adding water (2.46 mL), sodium hydroxide solution (10%, 2.46 mL), and water (7.38 mL) sequentially. The resulting mixture was filtered and concentrated under vacuum. The residue was purified by silica gel chromatography with dichloromethane/methanol (10/1) as the eluent to give **49** (1.5 g, 18%) as a yellow gum. ^{1}H NMR (600 MHz, $CDCl_3$): δ 7.08−6.88 (m, 2H), 6.85−6.72 (m, 1H), 4.82 (d, J = 6.9 Hz, 1H), 4.50 (bs, 3H), 3.77 (d, J = 6.4 Hz, 2H), 3.18−3.00 (m, 1H), 3.00−2.83 (m, 1H), 1.94−1.82 (m, 3H), 1.82−1.76 (m, 2H), 1.76−1.70 (m, 2H), 1.70−1.65 (m, 1H), 1.33−1.22 (m, 2H), 1.22−1.13 (m, 1H), 1.07−0.94 (ddd, J = 2.4, 12.2, 24.1 Hz, 2H). ^{13}C NMR (150 MHz, $CDCl_3$): δ 151.8 (d, J = 244.8 Hz), 147.3 (d, J = 10.6 Hz), 141.1 (d, J = 3.1 Hz), 117.6 (d, J = 6.8 Hz), 115.7 (d, J = 18.4 Hz), 112.3 (d, J = 1.0 Hz), 74.9, 74.0, 39.6, 38.6, 37.8, 29.9, 26.5, 25.8. ^{19}F (565 MHz, $CDCl_3$): δ −136.8 to −136.95 (m). HRMS (ESI): calcd for $C_{16}H_{24}FNO_2$ $[M + H]^+$, 282.1869; found, 282.1862.

*3-Amino-1-(3-(cyclohexylmethoxy)-5-fluorophenyl)propan-1-ol (**50**).* The general procedure was followed with nitrile **41** (5 g, 35.6 mmol, 1.1 *eq*) yielding a yellow gum (1.60 g, 51%). ^{1}H NMR (600 MHz, $CDCl_3$): δ 6.73−6.68 (m, 1H), 6.65 (d, J = 9.3 Hz, 1H), 6.46 (dt, J = 2.2, 10.7 Hz, 1H), 4.87 (dd, J = 2.6, 8.4 Hz, 1H), 3.71 (d, J = 6.4 Hz, 2H), 3.29 (bs, 3H), 3.10−3.03 (m, 1H), 3.00−2.89 (m, 1H), 1.88−1.80 (m, 3H), 1.79−1.73 (m, 3H), 1.73−1.64 (m, 2H), 1.32−1.24 (m, 2H), 1.23−1.15 (m, 1H), 1.03 (ddd, J = 3.2, 12.3, 24.3 Hz, 2H). ^{13}C NMR (150 MHz, $CDCl_3$): δ 163.6 (d, J = 244.3 Hz), 160.6 (d, J = 11.2 Hz), 148.47 (d, J = 8.6 Hz), 117.6 (d, J = 1.9 Hz), 104.6 (d, J = 22.2 Hz), 100.6 (d, J = 25.0 Hz), 74.8, 73.8, 40.3, 39.2, 37.7, 29.9, 26.6, 25.8. ^{19}F (565 MHz, $CDCl_3$): δ −112.20 (t, J = 10.1 Hz). HRMS (ESI): calcd for $C_{16}H_{24}FNO_2$ $[M + H]^+$, 282.1869; found, 282.1874.

*3-Amino-1-(5-(cyclohexylmethoxy)-2-fluorophenyl)propan-1-ol (**51**).* The general procedure was followed with compound **42** (3.5 g, 12.6 mmol, 1 equiv) giving a yellow gum (800 mg, 22%) ^{1}H NMR (600 MHz, $CDCl_3$): δ 7.11 (dd, J = 3.1, 6.0 Hz, 1H), 6.87 (dd, J = 9.0, 9.7 Hz, 1H), 6.69 (dt, J = 3.6, 9.0 Hz, 1H), 5.20 (dd, J = 3.0, 8.4 Hz, 1H), 3.75−3.69 (m, 2H), 3.47−2.98 (m, 4H), 2.98−2.94 (m, 1H), 1.94−1.88 (m, 1H), 1.87−1.82 (m, 2H), 1.80−1.72 (m, 4H), 1.70−1.66 (m, 1H), 1.32−1.24 (m, 2H), 1.23−1.15 (m, 1H), 1.03 (ddd, J = 3.3, 12.3, 24.2 Hz, 2H). ^{13}C NMR (150 MHz, $CDCl_3$): δ 155.7 (d, J = 1.7 Hz), 153.6 (d, J = 237.4 Hz), 132.8 (d, J = 14.9 Hz), 115.5 (d, J = 23.5 Hz), 113.9 (d, J = 8.0 Hz), 112.7 (d, J = 4.5 Hz), 74.2, 69.5 (d, J = 1.6 Hz), 40.5, 38.1, 37.9, 30.0, 30.0, 26.6, 25.9. ^{19}F (565 MHz, $CDCl_3$): δ −130.78 to −130.88 (m). HRMS (ESI): calcd for $C_{16}H_{24}FNO_2$ $[M + H]^+$, 282.1869; found, 282.1864.

*3-Amino-1-(3-(cyclohexylmethoxy)-2-fluorophenyl)propan-1-ol (**52**).* The general procedure was followed using nitrile **43** (3 g, 10.8

https://doi.org/10.1021/acs.jmedchem.1c00279
J. Med. Chem. 2021, 64, 8287−8302

mmol, 1 equiv) resulting in the isolation of a yellow gum (2.1 g, 66%). ^{1}H NMR (600 MHz, $CDCl_3$): δ 7.1 (t, J = 6.7 Hz, 1H), 7 (t, J = 8.0 Hz, 1H), 6.82 (t, J = 8.0 Hz, 1H), 5.25 (d, J = 8.3 Hz, 1H), 4.25 (bs, 3H), 3.77 (d, J = 6.3 Hz, 2H), 3.15−3.06 (m, 1H), 3.06−2.96 (m, 1H), 2.00−1.95 (m, 1H), 1.89−1.84 (m, 3H), 1.83−1.79 (m, 1H), 1.76−1.72 (m, 2H), 1.7−1.66 (m, 1H), 1.32−1.24 (m, 2H), 1.22−1.14 (m, 1H), 1.07−1.00 (ddd, J = 3.3, 12.4, 24.2 Hz, 2H). ^{13}C NMR (150 MHz, $CDCl_3$): δ 149.4 (d, J = 244.7 Hz), 147.1 (d, J = 10.7 Hz), 132.6 (d, J = 10.7 Hz), 123.8 (d, J = 4.3 Hz), 118.4 (d, J = 3.2 Hz), 113.4, 74.9, 68.7, 39.8, 37.7, 37.1, 29.1, 26.6, 25.8. ^{19}F (565 MHz, $CDCl_3$): δ −141.76 to −141.84 (m). HRMS (ESI): calcd for $C_{16}H_{24}FNO_2$ $[M + H]^+$, 282.1869; found, 282.1869.

*3-Amino-1-(4-fluoro-3-((2,6,6-trimethylcyclohex-1-en-1-yl)-methoxy)phenyl)propan-1-ol (**53**).* Steps were carried out according to the general procedure using compound **44** (6 g, 18.9 mmol, 1 equiv) to give title compound **53** (1.40 g, 22%) as a yellow gum. ^{1}H NMR (600 MHz, $CDCl_3$): δ 7.12 (dd, J = 1.54, 8.0 Hz, 1H), 6.99 (dd, J = 8.3, 11.0 Hz, 1H), 6.87−6.81 (m, 1H), 4.90 (dd, J = 2.2, 8.8 Hz, 1H), 4.50 (s, 2H), 3.62 (bs, 3H), 3.15−3.06 (m, 1H), 3.01−2.91 (m, 1H), 2.03 (t, J = 6.2 Hz, 2H), 1.89−1.82 (m, 1H), 1.78−1.74 (m, 1H), 1.72 (s, 3H), 1.66−1.61 (m, 2H), 1.53−1.45 (m, 2H), 1.05 (s, 6H). ^{13}C NMR (150 MHz, $CDCl_3$): δ 152.1 (d, J = 244.6 Hz), 147.3 (d, J = 11.1 Hz), 141.4 (d, J = 3.3 Hz), 136.2, 132.9, 118.07 (d, J = 6.7 Hz), 115.7 (d, J = 18.6 Hz), 113.2 (d, J = 1.9 Hz), 74.9, 66.4, 40.4, 39.4, 39.3, 34.1, 33.0, 28.5, 19.9, 19.3. ^{19}F (565 MHz, $CDCl_3$): δ −135.72 to −135.82 (m). HRMS (ESI): calcd for $C_{19}H_{28}FNO_2$ $[M + H]^+$, 322.2182; found, 322.2176.

*3-Amino-1-(3-fluoro-5-((2,6,6-trimethylcyclohex-1-en-1-yl)-methoxy)phenyl)propan-1-ol (**54**).* Utilizing the general procedure with compound **45** (6 g, 18.9 mmol, 1 equiv) led to the successful isolation of a yellow gum (1.50 g, 18%). ^{1}H NMR (600 MHz, $CDCl_3$): δ 6.82−6.72 (m, 1H), 6.70−6.62 (m, 1H), 6.57−6.50 (m, 1H), 4.88 (dd, J = 2.5, 8.4 Hz, 1H), 4.59 (bs, 3H), 4.39 (s, 2H), 3.18−3.06 (m, 1H), 3.06−2.84 (m, 1H), 2.07−2.00 (m, 2H), 1.97−1.86 (m, 1H), 1.83−1.75 (m, 1H), 1.67 (s, 3H), 1.66−1.56 (m, 2H), 1.53−1.42 (m, 2H), 1.02 (s, 6H). ^{13}C NMR (150 MHz, $CDCl_3$): δ 163.6 (d, J = 242.9 Hz), 160.7 (d, J = 10.6 Hz), 148.0 (d, J = 8.4 Hz), 136.1, 132.8, 107.8 (d, J = 1.4 Hz), 104.7 (d, J = 22.7 Hz), 100.9 (d, J = 24.8 Hz), 74.1, 64.9, 39.6, 39.3, 38.2, 34.1, 32.9, 28.5, 19.9, 19.3. ^{19}F (565 MHz, $CDCl_3$): δ −111.89 (t, J = 9.9 Hz). HRMS (ESI): calcd for $C_{19}H_{28}FNO_2$ $[M + H]^+$, 322.2182; found, 322.2173.

*3-Amino-1-(2-fluoro-5-((2,6,6-trimethylcyclohex-1-en-1-yl)-methoxy)phenyl)propan-1-ol (**55**).* The general procedure was carried out with **46** (3.0 g, 9.45 mmol, 1 equiv) giving amine **55** (1.1 g, 34%) as a yellow gum. ^{1}H NMR (600 MHz, $CDCl_3$): δ 7.18 (dd, J = 3.0, 5.8 Hz, 1H), 6.88 (t, J = 9.4 Hz, 1H), 6.79−6.75 (m, 1H), 5.22 (dd, J = 2.0, 8.3 Hz, 1H), 4.42 (d, J = 9.7 Hz, 1H), 4.38 (d, J = 9.7 Hz, 1H), 4.14 (bs, 3H), 3.16−3.06 (m, 1H), 3.06−2.95 (m, 1H), 2.03 (t, J = 5.9 Hz, 2H), 1.99−1.93 (m, 1H), 1.82−1.76 (m, 1H), 1.69 (s, 3H), 1.66−1.61 (m, 2H), 1.53−1.45 (m, 2H), 1.03 (s, 6H). ^{13}C NMR (150 MHz, $CDCl_3$): δ 155.8 (d, J = 1.4 Hz), 153.7 (d, J = 237.4 Hz), 135.7, 133.2, 132.6 (d, J = 14.8 Hz), 115.5 (d, J = 23.7 Hz), 114.4 (d, J = 7.9 Hz), 112.8 (d, J = 4.4 Hz), 69.1, 65.2, 40.1, 39.3, 37.4, 34.2, 32.9, 28.5, 28.5, 19.9, 19.4. ^{19}F (565 MHz, $CDCl_3$): δ −130.41 to −130.48 (m). HRMS (ESI): calcd for $C_{19}H_{28}FNO_2$ $[M + H]^+$, 322.2182; found, 322.2179.

*3-Amino-1-(2-fluoro-3-((2,6,6-trimethylcyclohex-1-en-1-yl)-methoxy)phenyl)propan-1-ol (**56**).* The actions of the general procedure were carried out with nitrile **47** (6.5 g, 20.5 mmol, 1 equiv) to give a brown gum (1.06 g, 16%). ^{1}H NMR (600 MHz, $CDCl_3$): δ 7.14 (t, J = 6.8 Hz, 1H), 7.04 (t, J = 8.0 Hz, 1H), 6.94 (t, J = 8.0 Hz, 1H), 5.24 (d, J = 7.2 Hz, 1H), 4.48 (d, J = 9.8 Hz, 1H), 4.45 (d, J = 9.8 Hz, 1H), 4.24 (bs, 3H), 3.12−3.03 (m, 1H), 3.03−2.92 (m, 1H), 2.03 (t, J = 6.0 Hz, 2H), 1.99−1.92 (m, 1H), 1.86−1.78 (m, 1H), 1.72 (s, 3H), 1.66−1.60 (m, 2H), 1.52−1.46 (m, 2H), 1.05 (s, 6H). ^{13}C NMR (150 MHz, $CDCl_3$): δ 149.8 (d, J = 244.3 Hz), 147.1 (d, J = 11.2 Hz), 136.1, 133.0, 132.9 (d, J = 11.1 Hz), 123.8 (d, J = 4.2 Hz), 118.9 (d, J = 3.2 Hz), 114.5, 68.7, 66.5, 39.9, 39.3, 37.4, 34.1, 33.0, 28.5, 19.9, 19.3. ^{19}F (565 MHz, $CDCl_3$): δ −140.35 to −140.46 (m). HRMS (ESI): calcd for $C_{19}H_{28}FNO_2$ $[M + H]^+$, 322.2182; found, 322.2173.

*3-Amino-1-(3-((4,4-difluorocyclohexyl)methoxy)phenyl)propan-1-ol (**57**).* Using compound **48** (3.0 g, 10.1 mmol, 1 equiv) and following the general procedure gave amine **57** (580 mg, 17% yield) as a yellow gum. ^{1}H NMR (600 MHz, $CDCl_3$): δ 7.19 (t, J = 7.9 Hz, 1H), 6.92−6.89 (m, 1H), 6.89−6.86 (m, 1H), 6.74 (dd, J = 2.0, 8.2 Hz, 1H), 5.80 (bs, 4H), 4.84 (dd, J = 2.6, 9.0 Hz, 1H), 3.76 (d, J = 6.3 Hz, 2H), 3.12−3.04 (m, 1H), 3.01−2.94 (m, 1H), 2.15−2.07 (m, 2H), 1.97−1.86 (m, 4H), 1.84−1.81 (m, 1H), 1.81−1.64 (m, 2H), 1.43−1.35 (m, 2H). ^{13}C NMR (150 MHz, $CDCl_3$): δ 159.2, 146.3, 129.5, 123.6 (t, J = 240.0 Hz), 118.0, 113.2, 111.8, 73.2, 71.8, 38.8, 37.4, 36.0, 33.2 (dd, J = 23.2, 24.7 Hz), 25.9, 25.8. ^{19}F (565 MHz, $CDCl_3$): δ −91.39 (d, J = 235.8 Hz), −101.99 (d, J = 235.8 Hz). HRMS (ESI): calcd for $C_{16}H_{23}F_2NO_2$ $[M + H]^+$, 300.1775; found, 300.1761.

*3-Amino-1-(3-(cyclohexylmethoxy)phenyl)propan-3,3-d_2-1-ol (**58**).* 3-(3-(Cyclohexylmethoxy) phenyl)-3-hydroxypropanenitrile[19] (200 mg, 0.77 mmol) was reduced with LAD (100 mg, 2.38 mmol). Following the common workup procedure, the crude product was purified by FC (silica, 70:30:0−90:10:4−70:30:4 DCM/MeOH/NH_4OH) giving **58** as yellow oil (69 mg, 34%). ^{1}H NMR (500 MHz, $CDCl_3$): δ 7.23 (t, J = 7.9 Hz, 1H), 6.96 (s, 1H), 6.91 (d, J = 7.6 Hz, 1H), 6.77 (dd, J = 8.4, 2.6 Hz, 1H), 4.94 (dd, J = 8.6, 3.2 Hz, 1H), 3.76 (d, J = 6.4 Hz, 2H), 2.45 (s, 3H), 1.91−1.82 (m, 3H), 1.79−1.65 (m, 5H), 1.35−1.14 (m, 3H), 1.05 (qd, J = 12.2, 3.4 Hz, 2H). ^{13}C NMR (126 MHz, $CDCl_3$): δ 159.6, 146.9, 129.3, 117.8, 113.2, 111.8, 75.6, 73.5, 39.5, 37.9, 30.1, 26.6, 25.9. HRMS (ESI): m/z calcd for $C_{16}H_{24}D_2NO_2$ $[M + H]^+$ 266.2084; found, 266.2083.

*3-Amino-1-(3-((4,4-difluorocyclohexyl)methoxy)phenyl)propan-3,3-d_2-1-ol (**59**).* The general procedure for the reduction of nitrile was followed using nitrile **48** (200 mg, 0.77 mmol) and LAD (100 mg, 2.38 mmol). Following purification by FC (silica, 90:10:0−70:30:0−90:10:4−70:30:4 DCM/MeOH/NH_4OH) gave **59** as a colorless syrup (140 mg, 45%). ^{1}H NMR (500 MHz, $CDCl_3$): δ 7.23 (d, J = 7.8 Hz, 1H), 6.97 (s, 1H), 6.93 (d, J = 7.6 Hz, 1H), 6.77 (dd, J = 8.1, 2.5 Hz, 1H), 4.95 (dd, J = 8.7, 3.0 Hz, 1H), 3.83 (dd, J = 6.5, 2.1 Hz, 2H), 2.18−2.10 (m, 3H), 2.00−1.93 (m, 4H), 1.92−1.84 (m, 4H), 1.81−1.66 (m, 5H), 1.47−1.38 (m, 2H). ^{13}C NMR (126 MHz, $CDCl_3$): δ 159.2, 147.1, 129.4, 118.2, 113.2, 111.7, 75.6, 71.8 (d, J = 2.8 Hz), 39.5, 36.1, 33.2 (dd, J = 25.5, 22.8 Hz), 25.9 (d, J = 9.7 Hz). ^{19}F NMR (471 MHz, $CDCl_3$): δ −91.40 (d, J = 236.4 Hz), −102.00 (d, J = 236.2 Hz). HRMS (ESI): m/z calcd for $C_{16}H_{21}D_2F_2NO_2$ $[M]^+$, 301.1820; found, 301.1822.

RPE65 Crystallization and Structure Determination. Crystals of RPE65 in the complex with 4-fluoro-emixustat (**49**), C-2′-fluoro-MB-004 (**24**), or C-4 *gem*-difluoro-emixustat (**57**) were obtained using previously described procedures.[32,33] Briefly, isolated bovine RPE membranes were incubated with 1 mM of each compound [delivered in dimethylformamide (DMF)] for 15 min prior to solubilization with 24 mM hexaethylene glycol monooctyl ether (C_8E_6). After anion-exchange chromatography, purified RPE65 was concentrated to 10−15 mg/mL and the test compounds were again to a concentration of 1 mM prior to crystallization. An RPE65 sample was also prepared in the absence of added inhibitors. Crystals were grown by the hanging-drop vapor-diffusion method by mixing 2 μL of a 10 mg/mL RPE65 sample with 2 μL of one of the following crystallization solutions: 100 mM 2-(cyclohexylamino)ethanesulfonic acid−NaOH, pH 9.5, containing 40% (v/v) polyethylene glycol 300 and 200 mM NaCl, which was used for the samples containing **49** or no added inhibitor, or 100 mM Tris−HCl, pH 8.5, containing 30% (v/v) polyethylene glycol 200 and 200 mM ammonium phosphate dibasic, which was used for the samples containing **24** or **57**. In both cases, the drops were incubated in a well solution consisting of 100 mM 2-(cyclohexylamino)ethanesulfonic acid−NaOH, pH 9.5, containing 40% (v/v) polyethylene glycol 300 and 200 mM NaCl at 8 °C. Crystals of approximately 100 × 100 × 300 μm in size were obtained after 1−2 weeks of incubation. Mature crystals were harvested directly into liquid nitrogen for X-ray data collection.

https://doi.org/10.1021/acs.jmedchem.1c00279
J. Med. Chem. 2021, 64, 8287−8302

X-ray diffraction data were collected at the SSRL 12−2, the APS NE-CAT 24-ID-E, or the NSLS-II FMX beamlines. Data were processed using XDS,[62] and the initial model was obtained by direct refinement using published RPE65 coordinates in which ligands had been removed[32] (PDB accession codes: 4RSE and 4RSC). The structures were refined by alternating reciprocal space refinement in REFMAC[63] and manual building and adjustments in Coot.[64] Ligand coordinates and geometry dictionary files were generated using the Grade server (http://grade.globalphasing.org/cgi-bin/grade/server.cgi). The models were validated using MolProbity[65] and the wwPDB validation server.[66]

RPE65 Retinoid Isomerase Activity Assay. Primary amine listed in Tables 1 and 2 and Supporting Information Table S1 in DMF (1 μL) was added to a suspension containing 300 μg of RPE microsomal proteins, 1% bovine serum albumin, 2 mM disodium pyrophosphate, and 25 μM human apo-cellular retinaldehyde-binding protein (CRALBP) in 10 mM BTP buffer (200 μL) to a final concentration from 0 to 2 μM. After incubation at room temperature for 5 min, the resulting mixture was mixed with half microliter of all-*trans*-retinol (5 mM) in DMF and then incubated at 37 °C for 1 h. The reaction was quenched by adding 400 μL of methanol (Fisher Chemical, Fair Lawn, NJ), and the products were extracted with 400 μL of hexanes. Production of 11-*cis*-retinol was quantified by normal-phase HPLC using a Zorbax Rx-SIL column (5 μm, 4.6 × 250 mm, Agilent, Santa Clara, CA) with 10% (v/v) ethyl acetate in hexanes as the eluent at a flow rate of 1.4 mL·min^{-1}. Retinoids were detected by monitoring their absorbance at 325 nm and quantified based on a standard curve representing the relationship between the amount of 11-*cis*-retinol and the area under the corresponding chromatographic peak.

Quantification of Representative Primary Amine Compound Levels in the Serum and Eyes of Mice after Treatments. 8-week-old BL/6J mice were treated with a 380 nmol visual cycle modulator **24**, **49**, **57**, **58**, **59**, or emixustat in dimethyl sulfoxide (50 μL) by intraperitoneal injection and sacrificed at 3 h, 1 day, or 7 days later. Blood and eyeball samples were collected immediately. After clotting at room temperature for 30 min, the blood samples were centrifuged for 10 min at 17,000*g* in a temperature-controlled benchtop centrifuge (Eppendorf AG). Each serum sample (100 μL) was carefully removed to avoid disturbing loose clots, precipitated with 400 μL of pre-cooled methanol, and centrifuged at 17,000*g* for 15 min at 4 °C. The supernatant was carefully transferred to a SpinX centrifuge tube filter with a 0.45 μm cellulose acetate membrane (Costar, Salt Lake City, UT) and centrifuged at 7000*g* for 2 min. The filtered samples were dried under vacuum, reconstituted in 100 μL of 50% methanol/water, and centrifuged at 17,000*g* for 15 min at 4 °C. The resulting supernatants were ready for LC/MS analyses. The two eyeballs from each mouse were homogenized in acetonitrile (2 × 800 μL). The resulting mixture was centrifuged at 17,000*g* for 15 min at 4 °C. The supernatant was dried under vacuum, reconstituted in 100 μL of 50% methanol/water, and centrifuged at 17,000*g* for 15 min at 4 °C. Twenty microliters of the supernatant extracted from the serum or eye samples was injected into an Ultimate 3000 HPLC system coupled with a LXQ mass spectrometer (ThermoFisher Scientific, Waltham, MA) with an ESI unit. The separation was performed on a Proshell EC-18 column (2.7 μm, 3.0 × 150 mm, Agilent, Santa Clara, CA) using a mobile phase consisting of 0.1% aqueous formic acid (A) and acetonitrile (B) at a flow rate of 600 μL·min^{-1}, and the mobile-phase gradients and time course were as follows: 0−2 min, 95% A/5% B; 2−10 min, 95−15% A/5−85% B. The signals were detected in the selected reaction monitoring mode under conditions described in Supporting Information Table S3 and quantified based on the standard curves representing the relationship between the amounts of primary amine standards and the areas under the corresponding chromatographic peaks.

VAP-1 Oxidation Assay. Mouse aorta homogenates were used as the source of VAP-1 for this study. Aortas were removed from mice (4−6 weeks old) that had been euthanized by CO_2 asphyxiation followed by cervical dislocation. The aorta was dissected and the blood was removed by rinsing the tissue with phosphate-buffered saline. Aorta samples were used immediately or stored at −80 °C until needed. Two aortas were minced using a stainless-steel single-edge blade and homogenized in a KONTES Potter-Elvehjem tissue grinder/homogenizer glass pestle in 1 mL of 10 mM HEPES-NaOH, pH 7.6. The homogenate was collected into a 1.5 mL Eppendorf tube. Five μl of a 20 mM ethanolic stock solution of emixustat or d_2-emixustat (**58**) was added to the aorta homogenate to give a final substrate concentration of 100 μM. The sample was mixed and then incubated at 28 °C with 300 rpm shaking in an Eppendorf Thermomixer. 200 μL samples were taken at 0, 1, and 2 h after the initiation of the reaction. At each time point, the reactions were immediately quenched with 100 μL of 100% MeOH, vortexed for 3 s, and stored at −20 °C. After samples from all time points were collected and frozen, the samples were thawed and centrifuged at 15,000 rpm for 10 min; 250 μL of each supernatant was collected, placed into a borosilicate tube, and dried in a Speedvac rotoevaporator. Each dried sample was redissolved in 300 μL of a 1:1 MeOH/H_2O solution, centrifuged to remove particulates, and then transferred to an HPLC vial. 50 μL of the sample was used for analysis on an Agilent 1260 Infinity series HPLC equipped with a Proshell EC-18 column and a diode array detector. The sample was separated using a mobile phase consisting of 0.1% (v/v) formic acid in H_2O and acetonitrile at the following ratios and time intervals: 95:5 for 2 min, a gradient from 95:5 to 15:85 over 8 min, a gradient from 15:85 to 2:98 over 0.5 min, continued 2:98 for 4 min, and then a gradient from 2:98 to 95:5 over 0.5 min. The reaction substrate and product were assessed by monitoring absorbance at 275 nm. Emixustat and d_2-emixustat were eluted at ∼8.5 min, while the assay product (ACU-5201) was eluted at ∼13.25 min. A dilution series of known concentrations of authentic ACU-5201 in 1:1 MeOH/H_2O was run to generate a standard curve and facilitate the conversion of product AUCs to absolute mass.

■ ASSOCIATED CONTENT

Supporting Information

The Supporting Information is available free of charge at https://pubs.acs.org/doi/10.1021/acs.jmedchem.1c00279.

SMILES data and RPE65 EC_{50} values for compounds (CSV)

Synthesis and characterization of compounds, copies of NMR spectra, purity HPLC traces for the final synthesized compounds and intermediates, inhibition of RPE65-mediated isomerization reaction, detection of primary amines by mass spectroscopy, details of quantum chemical calculations, and X-ray data collection, processing, and refinement (PDF)

Accession Codes

The X-ray crystallography data sets reported in this article have been deposited in the Protein Data Bank [ID codes: 7K88 (C8E6 complex), 7K89 (compound **49** complex), 7K8G (compound **24** complex), and 7L0E (compound **57** complex)].

■ AUTHOR INFORMATION

Corresponding Authors

Arie Gruzman − *Department of Chemistry, Faculty of Exact Sciences, Bar-Ilan University, Ramat-Gan 5290002, Israel;* orcid.org/0000-0002-8006-4201; Email: Aric-Lev.Gruzman@biu.ac.il

Gregory P. Tochtrop − *Department of Chemistry, Case Western Reserve University, Cleveland, Ohio 44106, United States*; Email: gpt6@case.edu

Philip D. Kiser − *Department of Ophthalmology, Gavin Herbert Eye Institute and Department of Physiology and Biophysics, University of California, Irvine, California 92697,*

United States; Research Service, VA Long Beach Healthcare System, Long Beach, California 90822, United States; orcid.org/0000-0003-1184-9539; Email: pkiser@uci.edu

Krzysztof Palczewski − *Department of Ophthalmology, Gavin Herbert Eye Institute, Department of Physiology and Biophysics, and Department of Chemistry, University of California, Irvine, California 92697, United States;* orcid.org/0000-0002-0788-545X; Phone: (949)824-6527; Email: kpalczew@uci.edu

Authors

Eliav Blum − *Department of Chemistry, Faculty of Exact Sciences, Bar-Ilan University, Ramat-Gan 5290002, Israel;* orcid.org/0000-0003-1933-6367

Jianye Zhang − *Department of Ophthalmology, Gavin Herbert Eye Institute, University of California, Irvine, California 92697, United States;* orcid.org/0000-0002-9579-1399

Jordan Zaluski − *Department of Chemistry, Case Western Reserve University, Cleveland, Ohio 44106, United States;* orcid.org/0000-0002-2563-8807

David E. Einstein − *Department of Physiology and Biophysics, University of California, Irvine, California 92697, United States; Research Service, VA Long Beach Healthcare System, Long Beach, California 90822, United States;* orcid.org/0000-0003-1584-4049

Edward E. Korshin − *Department of Chemistry, Faculty of Exact Sciences, Bar-Ilan University, Ramat-Gan 5290002, Israel*

Adam Kubas − *Institute of Physical Chemistry, Polish Academy of Sciences, Warsaw 01-224, Poland;* orcid.org/0000-0002-5508-0533

Complete contact information is available at: https://pubs.acs.org/10.1021/acs.jmedchem.1c00279

Author Contributions

$^{\nabla}$E.B. and J.Z. contributed equally to the conduct of the study and development of the manuscript.

Notes

The authors declare no competing financial interest.

■ ACKNOWLEDGMENTS

This study was supported by a Bar-Ilan University new faculty grant (to A.G.). K.P. is the Irving H. Leopold Chair of Ophthalmology at the Gavin Herbert Eye Institute, Department of Ophthalmology, University of California, Irvine. This research was supported in part by grants to K.P. from the National Institutes of Health (NIH) (EY009339, EY027283, and EY030873); to P.D.K. from the U.S. Department of Veterans Affairs (I01BX004939); and to G.P.T. from the National Science Foundation (NSF-CHE Award no. 1904530) and the Department of Defense (DOD-CDMRP award no. W81XWH-16-1-0699). The authors also acknowledge support from an RPB unrestricted grant to the Department of Ophthalmology, University of California, Irvine. The authors also thank the Interdisciplinary Center for Mathematical and Computational Modeling in Warsaw, Poland, under grant GB79-5, for granting access to high-performance computing resources.

■ ABBREVIATIONS

A2E, *N*-retinylidene-*N*-retinylethanolamine; AMD, age-related macular degeneration; C_8E_6, hexaoxyethylene monooctyl ether; CRALBP, cellular retinaldehyde-binding protein; DLPNO-CCSD(T), domain-based local pair natural orbital coupled-cluster with single, double, and perturbative triple excitation; ETS, transition-state theory; KIE, kinetic isotope effect; LED, local energy decomposition; NCI, noncovalent interaction; NOCV, natural orbitals for chemical valence; RPE65, retinoid isomerase; VAP-1, vascular adhesion protein-1.

■ REFERENCES

(1) Travis, G. H.; Golczak, M.; Moise, A. R.; Palczewski, K. Diseases caused by defects in the visual cycle: retinoids as potential therapeutic agents. *Annu. Rev. Pharmacol. Toxicol.* **2007**, *47*, 469−512.

(2) Palczewski, K.; Kiser, P. D. Shedding new light on the generation of the visual chromophore. *Proc. Natl. Acad. Sci. U. S. A.* **2020**, *117*, 19629−19638.

(3) Sparrow, J. R.; Gregory-Roberts, E.; Yamamoto, K.; Blonska, A.; Ghosh, S. K.; Ueda, K.; Zhou, J. The bisretinoids of retinal pigment epithelium. *Prog. Retin. Eye Res.* **2012**, *31*, 121−135.

(4) Sparrow, J. R. Bisretinoids of RPE lipofuscin: trigger for complement activation in age-related macular degeneration. *Adv. Exp. Med. Biol.* **2010**, *703*, 63−74.

(5) Golczak, M.; Kuksa, V.; Maeda, T.; Moise, A. R.; Palczewski, K. Positively charged retinoids are potent and selective inhibitors of the trans-cis isomerization in the retinoid (visual) cycle. *Proc. Natl. Acad. Sci. U. S. A.* **2005**, *102*, 8162−8167.

(6) Kubota, R.; Birch, D. G.; Gregory, J. K.; Koester, J. M. Randomised study evaluating the pharmacodynamics of emixustat hydrochloride in subjects with macular atrophy secondary to Stargardt disease. *Br. J. Ophthalmol.* **2020**, *0*, 1−6.

(7) Kubota, R.; Jhaveri, C.; Koester, J. M.; Gregory, J. K. Effects of emixustat hydrochloride in patients with proliferative diabetic retinopathy: a randomized, placebo-controlled phase 2 study. *Graefes Arch. Clin. Exp. Ophthalmol.* **2021**, *259*, 369−378.

(8) Kubota, R.; Gregory, J.; Henry, S.; Mata, N. L. Pharmacotherapy for metabolic and cellular stress in degenerative retinal diseases. *Drug Discov. Today* **2020**, *25*, 292−304.

(9) Kubota, R.; Calkins, D. J.; Henry, S. H.; Linsenmeier, R. A. Emixustat reduces metabolic demand of dark activity in the retina. *Invest. Ophthalmol. Vis. Sci.* **2019**, *60*, 4924−4930.

(10) Rosenfeld, P. J.; Dugel, P. U.; Holz, F. G.; Heier, J. S.; Pearlman, J. A.; Novack, R. L.; Csaky, K. G.; Koester, J. M.; Gregory, J. K.; Kubota, R. Emixustat Hydrochloride for Geographic Atrophy Secondary to Age-Related Macular Degeneration. *Ophthalmology* **2018**, *125*, 1556−1567.

(11) Bavik, C.; Henry, S. H.; Zhang, Y.; Mitts, K.; McGinn, T.; Budzynski, E.; Pashko, A.; Lieu, K. L.; Zhong, S.; Blumberg, B.; Kuksa, V.; Orme, M.; Scott, I.; Fawzi, A.; Kubota, R. Visual cycle modulation as an approach toward preservation of retinal integrity. *PLoS One* **2015**, *10*, No. e0124940.

(12) Dugel, P. U.; Novack, R. L.; Csaky, K. G.; Richmond, P. P.; Birch, D. G.; Kubota, R. Phase ii, randomized, placebo-controlled, 90-day study of emixustat hydrochloride in geographic atrophy associated with dry age-related macular degeneration. *Retina* **2015**, *35*, 1173−1183.

(13) Kubota, R.; Al-Fayoumi, S.; Mallikaarjun, S.; Patil, S.; Bavik, C.; Chandler, J. W. Phase 1, dose-ranging study of emixustat hydrochloride (ACU-4429), a novel visual cycle modulator, in healthy volunteers. *Retina* **2014**, *34*, 603−609.

(14) Kubota, R.; Boman, N. L.; David, R.; Mallikaarjun, S.; Patil, S.; Birch, D. Safety and effect on rod function of ACU-4429, a novel small-molecule visual cycle modulator. *Retina* **2012**, *32*, 183−188.

(15) Reid, M. J.; Eyre, R.; Podoll, T. Oxidative Deamination of Emixustat by Human Vascular Adhesion Protein-1/Semicarbazide-Sensitive Amine Oxidase. *Drug Metab. Dispos.* **2019**, *47*, 504−515.

(16) Podoll, T.; Geisler, L.; Parys, M. V.; Hanson, G.; Reid, M. J. Validation and reproducibility of an LC-MS/MS method for

emixustat and its three deaminated metabolites in human plasma. *Bioanalysis* **2018**, *10*, 1803.
(17) Fitzsimmons, M. E.; Sun, G.; Kuksa, V.; Reid, M. J. Disposition, profiling and identification of emixustat and its metabolites in humans. *Xenobiotica* **2018**, *48*, 592−604.
(18) Miao, Z.; Farnham, J. G.; Hanson, G.; Podoll, T.; Reid, M. J. Bioanalysis of emixustat (ACU-4429) in whole blood collected with volumetric absorptive microsampling by LC-MS/MS. *Bioanalysis* **2015**, *7*, 2071−2083.
(19) Zhang, J.; Kiser, P. D.; Badiee, M.; Palczewska, G.; Dong, Z.; Golczak, M.; Tochtrop, G. P.; Palczewski, K. Molecular pharmacodynamics of emixustat in protection against retinal degeneration. *J. Clin. Invest.* **2015**, *125*, 2781−2794.
(20) Maeda, A.; Golczak, M.; Chen, Y.; Okano, K.; Kohno, H.; Shiose, S.; Ishikawa, K.; Harte, W.; Palczewska, G.; Maeda, T.; Palczewski, K. Primary amines protect against retinal degeneration in mouse models of retinopathies. *Nat. Chem. Biol.* **2011**, *8*, 170−178.
(21) Muller, K.; Faeh, C.; Diederich, F. Fluorine in pharmaceuticals: looking beyond intuition. *Science* **2007**, *317*, 1881−1886.
(22) Gillis, E. P.; Eastman, K. J.; Hill, M. D.; Donnelly, D. J.; Meanwell, N. A. Applications of fluorine in medicinal chemistry. *J. Med. Chem.* **2015**, *58*, 8315−8359.
(23) Gant, T. G. Using deuterium in drug discovery: leaving the label in the drug. *J. Med. Chem.* **2014**, *57*, 3595−3611.
(24) Jakubec, P.; Petráš, P.; Ďuriš, A.; Berkeš, D. The first example of a crystallization-induced asymmetric transformation (CIAT) in the Mannich reaction. *Tetrahedron: Asymmetry* **2010**, *21*, 69−74.
(25) Valachová, D.; Ferko, B.; Puchlová, E.; Caletková, O.; Berkeš, D.; Kolarovič, A.; Jakubec, P. Stereoselective Synthesis of syn-γ-Hydroxynorvaline and Related α-Amino Acids. *Synthesis* **2019**, *51*, 4568−4575.
(26) Cierna, M.; Markus, J.; Dohanosova, J.; Moncol, J.; Jakubec, P.; Berkes, D.; Caletkova, O. Stereoselective Mannich Reaction Driven by Crystallization. *Eur. J. Org. Chem.* **2020**, *2020*, 5685−5689.
(27) Lehmann, F.; Pilotti, Å.; Luthman, K. Efficient large scale microwave assisted Mannich reactions using substituted acetophenones. *Mol. Divers.* **2003**, *7*, 145−152.
(28) Wang, J.; Wang, Y.; Liu, D.; Zhang, W. Asymmetric Hydrogenation of β-Secondary Amino Ketones Catalyzed by a Ruthenocenyl Phosphino-oxazoline-ruthenium Complex (RuPHOX-Ru): the Synthesis of γ-Secondary Amino Alcohols. *Adv. Synth. Catal.* **2015**, *357*, 3262−3272.
(29) Ella-Menye, J.-R.; Sharma, V.; Wang, G. New synthesis of chiral 1,3-oxazinan-2-ones from carbohydrate derivatives. *J. Org. Chem.* **2005**, *70*, 463−469.
(30) Davies, S. G.; Haggitt, J. R.; Ichihara, O.; Kelly, R. J.; Leech, M. A.; Mortimer, A. J. P.; Roberts, P. M.; Smith, A. D. Asymmetric total synthesis of sperabillins B and D via lithium amide conjugate addition. *Org. Biomol. Chem.* **2004**, *2*, 2630−2649.
(31) Scott, I. L.; Kuksa, V.; Orme, M. W.; Little, T.; Gall, A.; Hong, F. Alkoxy compounds for disease treatment. U.S. Patent 8,829,244 B2, 2014..
(32) Kiser, P. D.; Zhang, J.; Badiee, M.; Li, Q.; Shi, W.; Sui, X.; Golczak, M.; Tochtrop, G. P.; Palczewski, K. Catalytic mechanism of a retinoid isomerase essential for vertebrate vision. *Nat. Chem. Biol.* **2015**, *11*, 409−415.
(33) Kiser, P. D.; Zhang, J.; Badiee, M.; Kinoshita, J.; Peachey, N. S.; Tochtrop, G. P.; Palczewski, K. Rational tuning of visual cycle modulator pharmacodynamics. *J. Pharmacol. Exp. Ther.* **2017**, *362*, 131−145.
(34) Scott, I. L.; Kuksa, V.; Orme, M. W.; Little, T.; Gall, A.; Hong, F. Preparation of alkoxybenzene compounds for disease treatment. *PCT Int. Appl.* **2009**, 0454479.
(35) Yu, P. H. Three types of stereospecificity and the kinetic deuterium isotope effect in the oxidative deamination of dopamine as catalyzed by different amine oxidases. *Biochem. Cell Biol.* **1988**, *66*, 853−861.
(36) Zhu, Q.; Sun, W.; Okano, K.; Chen, Y.; Zhang, N.; Maeda, T.; Palczewski, K. Sponge Transgenic Mouse Model Reveals Important Roles for the MicroRNA-183 (miR-183)/96/182 Cluster in Postmitotic Photoreceptors of the Retina*. *J. Biol. Chem.* **2011**, *286*, 31749−31760.
(37) Kiser, P. D.; Farquhar, E. R.; Shi, W.; Sui, X.; Chance, M. R.; Palczewski, K. Structure of RPE65 isomerase in a lipidic matrix reveals roles for phospholipids and iron in catalysis. *Proc. Natl. Acad. Sci. U. S. A.* **2012**, *109*, E2747−E2756.
(38) Golczak, M.; Kiser, P. D.; Lodowski, D. T.; Maeda, A.; Palczewski, K. Importance of membrane structural integrity for RPE65 retinoid isomerization activity. *J. Biol. Chem.* **2010**, *285*, 9667−9682.
(39) Sui, X.; Kiser, P. D.; Che, T.; Carey, P. R.; Golczak, M.; Shi, W.; von Lintig, J.; Palczewski, K. Analysis of carotenoid isomerase activity in a prototypical carotenoid cleavage enzyme, apocarotenoid oxygenase (ACO). *J. Biol. Chem.* **2014**, *289*, 12286−12299.
(40) Kloer, D. P.; Ruch, S.; Al-Babili, S.; Beyer, P.; Schulz, G. E. The structure of a retinal-forming carotenoid oxygenase. *Science* **2005**, *308*, 267−269.
(41) Redmond, T. M.; Poliakov, E.; Kuo, S.; Chander, P.; Gentleman, S. RPE65, Visual Cycle Retinol Isomerase, Is Not Inherently 11-cis-specific. *J. Biol. Chem.* **2010**, *285*, 1919−1927.
(42) Imai, Y. N.; Inoue, Y.; Nakanishi, I.; Kitaura, K. Cl-π interactions in protein-ligand complexes. *Protein Sci.* **2008**, *17*, 1129−1137.
(43) Jennings, W. B.; O'Connell, N.; Malone, J. F.; Boyd, D. R. An evaluation of substituent effects on aromatic edge-to-face interactions and CF-π versus CH-π interactions using an imino torsion balance model. *Org. Biomol. Chem.* **2013**, *11*, 5278−5291.
(44) Li, P.; Maier, J. M.; Vik, E. C.; Yehl, C. J.; Dial, B. E.; Rickher, A. E.; Smith, M. D.; Pellechia, P. J.; Shimizu, K. D. Stabilizing Fluorine-π Interactions. *Angew. Chem., Int. Ed.* **2017**, *56*, 7209−7212.
(45) Riplinger, C.; Neese, F. An efficient and near linear scaling pair natural orbital based local coupled cluster method. *J. Chem. Phys.* **2013**, *138*, 034106.
(46) Riplinger, C.; Sandhoefer, B.; Hansen, A.; Neese, F. Natural triple excitations in local coupled cluster calculations with pair natural orbitals. *J. Chem. Phys.* **2013**, *139*, 134101.
(47) Schneider, W. B.; Bistoni, G.; Sparta, M.; Saitow, M.; Riplinger, C.; Auer, A. A.; Neese, F. Decomposition of intermolecular interaction energies within the local pair natural orbital coupled cluster framework. *J. Chem. Theory Comput.* **2016**, *12*, 4778−4792.
(48) Johnson, E. R.; Keinan, S.; Mori-Sánchez, P.; Contreras-García, J.; Cohen, A. J.; Yang, W. Revealing noncovalent interactions. *J. Am. Chem. Soc.* **2010**, *132*, 6498−6506.
(49) Mitoraj, M.; Michalak, A. Natural orbitals for chemical valence as descriptors of chemical bonding in transition metal complexes. *J. Mol. Model.* **2007**, *13*, 347−355.
(50) Lin, Y.-S.; Li, G.-D.; Mao, S.-P.; Chai, J.-D. Long-range corrected hybrid density functionals with improved dispersion corrections. *J. Chem. Theory Comput.* **2013**, *9*, 263−272.
(51) Grimme, S.; Ehrlich, S.; Goerigk, L. Effect of the damping function in dispersion corrected density functional theory. *J. Comput. Chem.* **2011**, *32*, 1456−1465.
(52) Ziegler, T.; Rauk, A. On the calculation of bonding energies by the Hartree Fock Slater method. *Theor. Chim. Acta* **1977**, *46*, 1−10.
(53) Gong, B.; Boor, P. J. The role of amine oxidases in xenobiotic metabolism. *Expert Opin. Drug Metab. Toxicol.* **2006**, *2*, 559−571.
(54) Benedetti, M. S. Biotransformation of xenobiotics by amine oxidases. *Fundam. Clin. Pharmacol.* **2001**, *15*, 75−84.
(55) Claud, P.; Padovani, P.; Guichard, J. P.; Artur, Y.; Lainé, R. Involvement of semicarbazide-sensitive amine oxidase in tresperimus metabolism in human and in rat. *Drug Metab. Dispos.* **2001**, *29*, 735−741.
(56) Heuts, D. P. H. M.; Gummadova, J. O.; Pang, J.; Rigby, S. E. J.; Scrutton, N. S. Reaction of Vascular Adhesion Protein-1 (VAP-1) with Primary Amines. *J. Biol. Chem.* **2011**, *286*, 29584−29593.
(57) O'Leary, M. H. Multiple isotope effects on enzyme-catalyzed reactions. *Annu. Rev. Biochem.* **1989**, *58*, 377−401.

https://doi.org/10.1021/acs.jmedchem.1c00279
J. Med. Chem. 2021, 64, 8287−8302

(58) Northrop, D. B. The expression of isotope effects on enzyme-catalyzed reactions. *Annu. Rev. Biochem.* **1981**, *50*, 103−131.
(59) O'Leary, M. H. [4] Determination of heavy-aton isotope effects on enzyme-catalyzed reactions. *Methods Enzymol.* **1980**, *64*, 83−104.
(60) Schowen, K. B.; Schowen, R. L. The use of isotope effects to elucidate enzyme mechanisms. *Bioscience* **1981**, *31*, 826−831.
(61) Trifonov, L.; Afri, M.; Palczewski, K.; Korshin, E. E.; Gruzman, A. An Expedient Synthesis of CMF-019: (S)-5-Methyl-3-{1-(pentan-3-yl)-2- (thiophen-2-ylmethyl)-1H-benzo[d]imidazole-5-carboxamido}hexanoic Acid, a Potent Apelin Receptor (APJ) Agonist. *Med. Chem.* **2018**, *14*, 688−694.
(62) Kabsch, W. Integration, scaling, space-group assignment and post-refinement. *Acta Crystallogr. Sect. D Biol. Crystallogr.* **2010**, *66*, 133−144.
(63) Murshudov, G. N.; Skubák, P.; Lebedev, A. A.; Pannu, N. S.; Steiner, R. A.; Nicholls, R. A.; Winn, M. D.; Long, F.; Vagin, A. A. REFMAC5 for the refinement of macromolecular crystal structures. *Acta Crystallogr. Sect. D Biol. Crystallogr.* **2011**, *67*, 355−367.
(64) Emsley, P.; Lohkamp, B.; Scott, W. G.; Cowtan, K. Features and development ofCoot. *Acta Crystallogr. Sect. D Biol. Crystallogr.* **2010**, *66*, 486−501.
(65) Williams, C. J.; Headd, J. J.; Moriarty, N. W.; Prisant, M. G.; Videau, L. L.; Deis, L. N.; Verma, V.; Keedy, D. A.; Hintze, B. J.; Chen, V. B.; Jain, S.; Lewis, S. M.; Arendall, W. B., 3rd; Snoeyink, J.; Adams, P. D.; Lovell, S. C.; Richardson, J. S.; Richardson, D. C. MolProbity: More and better reference data for improved all-atom structure validation. *Protein Sci.* **2018**, *27*, 293−315.
(66) Read, R. J.; Adams, P. D.; Arendall, W. B., 3rd; Brunger, A. T.; Emsley, P.; Joosten, R. P.; Kleywegt, G. J.; Krissinel, E. B.; Lütteke, T.; Otwinowski, Z.; Perrakis, A.; Richardson, J. S.; Sheffler, W. H.; Smith, J. L.; Tickle, I. J.; Vriend, G.; Zwart, P. H. A new generation of crystallographic validation tools for the protein data bank. *Structure* **2011**, *19*, 1395−1412.

https://doi.org/10.1021/acs.jmedchem.1c00279
J. Med. Chem. 2021, 64, 8287−8302